NASA CONTRACTOR REPORT CR-187069

DATE: JANUARY 18, 1991

TO:

NASA-LEWIS RESEARCH CENTER
21000 BROOKPARK ROAD
CLEVELAND, OH 44135
SBIR-PHASE II CONTRACT #NAS3-25419

SBIR-01.03-3383 A
RELEASE DATE 05/03/93

"FIBER-OPTIC PHOTOELASTIC PRESSURE SENSORS FOR HIGH-TEMPERATURE GASES"

SBIR 1986 Phase II

PREPARED BY:

ALEX S. REDNER, P.E., PRESIDENT
PRINCIPAL INVESTIGATOR.
STRAINOPTIC TECHNOLOGIES, INC.
108 WEST MONTGOMERY AVENUE
NORTH WALES, PA 19454
TEL. (215) 661-0100 • FAX. (215) 699-7028

REF: STRAINOPTIC REPORT NO. 000195

TABLE OF CONTENTS

NASA
National Aeronautics and Space Administration

Report Documentation Page

1. Report No.	2. Government Accession No.	3. Recipient's Catalog No.
CR-187069		

4. Title and Subtitle	5. Report Date
"Fiber-Optic Photoelastic Pressure Sensors for High-Temperature Gases"	January 18, 1991
	6. Performing Organization Code

7. Author(s)	8. Performing Organization Report No.
Alex S. Redner, P.E.	000195
	10. Work Unit No.

9. Performing Organization Name and Address	11. Contract or Grant No.
Strainoptic Technologies, Inc. 108 West Montgomery Avenue North Wales, PA 19454	NAS3-25419
	13. Type of Report and Period Covered FINAL REPORT

12. Sponsoring Agency Name and Address	14. Sponsoring Agency Code
NASA-Lewis Research Center 21000 Brookpark Road Cleveland, OH 44135	

15. Supplementary Notes

16. Abstract

This report discusses work done on a passive optical sensor designed to measure high pressures (600 psi) with a gas side temperature of 1500° C. This work included material characterization for suitable birefringent material to operate up to 1500° C operation. Using a photoelastic model as a design tool, the sensor geometry was optimized. Housing seals and connecting fiber-optic cables were designed and tested. An electronic package (hardware and software) for operation of the birefringent sensor and for data acquisition was also developed. A series of tests were conducted to evaluate the design and durability of components and performance of the sensor. The result of this program is an optical sensor capable of measuring gas side temperatures up to 1500° C.

17. Key Words (Suggested by Author(s))	18. Distribution Statement
Fiber-Optic Pressure Sensor High-Temperature Birefringent Sensor	

19. Security Classif. (of this report)	20. Security Classif. (of this page)	21. No of pages	22. Price*
UNCL		66	

NASA FORM 1626 OCT 86

*For sale by the National Technical Information Service, Springfield, Virginia 22161

LIST OF SYMBOLS

$S = \sigma_1 - \sigma_2$	is the difference of principal stresses in the plane perpendicular to the light path.
t	is the length of the light path, thickness
C_B, C	Brewster constant, obtained by calibration
δ	retardation between wavefronts polarized in the direction of principal stresses.
I, Io	light intensity
P, A	Polarizer, Analyzer
T	temperature
α	coefficient of thermal expansion
D	is the diameter of the calibration specimen
F	is the applied force
σ	stress at a point
σ_m, σ_p	stress in the model or prototype
p	is the internal pressure
d	is the cylinder (or diaphragm) diameter
K	is a shape factor, function of the selected geometry
N	measured fringe order ($N = \delta/\lambda$)
	stress at the point of measurements (psi)
K_{ij}	coefficient obtained in curve fitting

SUMMARY - PHASE II RESEARCH

The purpose of the research and development reported here was to develop a PASSIVE-OPTICAL SENSOR FOR MEASURING GAS PRESSURE AT TEMPERATURES OF 1500° C.

The project was sponsored by NASA-LEWIS RESEARCH CENTER under the SBIR program, organized in two stages. The Phase I research project's objective was to demonstrate the feasibility of the concept. The Phase II research objective was to produce an operating prototype. The Phase II research project included:

-MATERIALS RESEARCH: Development and material characterization of a suitable birefringent sensor for 1500° C operation.

-TRANSDUCER ENGINEERING: Using a photoelastic model as a design tool, the sensor-geometry was optimized. The housing, seals, and connecting fiber-optic cable was designed and tested.

-ELECTRONIC READOUT SYSTEM DESIGN: An electronic package (hardware and software) were developed, for data acquisition using a birefringent sensor developed.

-TESTING: A series of tests were conducted in the research process, to evaluate the design, components, and final performance.

As a result of the R&D effort described in this report, a transducer capable of measuring 1500° C gas pressure was developed and tested, meeting the objectives of the project.

1. INTRODUCTION

The objective of the reported research work was to develop a passive optical sensor for measuring pressure of high-temperature gas, for use in control systems of modern aircraft engines.

The approach selected was to use a BIREFRINGENT (PHOTOELASTIC EFFECT) sensor. This choice was dictated by the following considerations:

a. Intrinsic vs. Extrinsic Fiber-Optic Sensor

In the "intrinsic" pessive optical sensor the sensing function takes place in the fiber itself. A large variety of devices based on this concept were tested, demonstrating that the environment can affect the fiber transmission. The fiber can respond to strain, temperature, magnetic field, and bending to name just a few.

An "extrinsic" sensor is not integral with the fiber. Here, a fiber-optic cable is used for transmission of the signal, but the modulation of the light is accomplished by an independent body, selected for optimum response to the measured quantity (pressure) and minimum noise. In this project, the EXTRINSIC concept was selected.

b. Birefringent Sensor

All transparent materials obey the BREWSTER LAW. When subjected to stress the material becomes birefringent, and its birefringence $n_1 - n_2$ is directly proportional to the stress:

$$n_1 - n_2 = \delta/t = (\sigma_1 - \sigma_2) \times C_B = S \times C_B \qquad (1)$$

where $S = \sigma_1 - \sigma_2$ is the difference of principal stresses in the plane perpendicular to the light path.

A stressed material placed in a path of polarized light will modulate the light; the attentuation (or transmittance) I/Io becomes:

In crossed polarizer arrangement $I/I_o = \sin^2 \pi\delta/\lambda$ (2a)
In parallel polarizer arrangement $I/I_o = \cos^2 \pi\delta/\lambda$ (2b)

An EXTRINSIC pressure sensor based on birefringence requires a suitable pressure-cavity geometry, developing high stress due to pressure, and very low stress due to other environments, such as acceleration, temperature, etc. Combining (1) and (2) above

$$I/I_o = \sin^2 \frac{\pi}{\lambda}(S \cdot C_B \cdot t)$$

with $S = f(P_i)$ (3)

The key consideration in developing a sensor for high-temperature gas was the temperature sensitivity and temperature response. Most of the commercially available transducers use electrical resistance (or capacitance) strain gage. These gages respond very strongly to the temperature and are temperature limited by the lead wires, attaching procedure, and most of all, by the temperature response of the gage.

The BIREFRINGENT SENSOR practically eliminates this problem. The birefringence is proportional to the difference of principal stresses (or strains) $\varepsilon_1 - \varepsilon_2$ and the sensor does not respond to equal strain in all directions, due to thermal expansions or temperature changes.

The results of the research reported confirms our assumption. Upon completion of the feasibility study Phase I, the research effort was channeled simultaneously along the following topics:

- Development and calibration of high-temperature optical materials
- Polarization of light at elevated temperature
- Fiber-optic links
- Design of the pressure transducer (sensor)
- Development of the readout system

In all these areas, the objectives were accomplished.

The prototype design was carriedout in two stages. In the first stage, a transducer operating at 600° C was tested at pressure 0-500 psi.

In the second stage, the concept was upgraded to permit the operation with gas temperature exceeding 1500° C. The transducer performed its function in accordance with its design. (See figure 1 below)

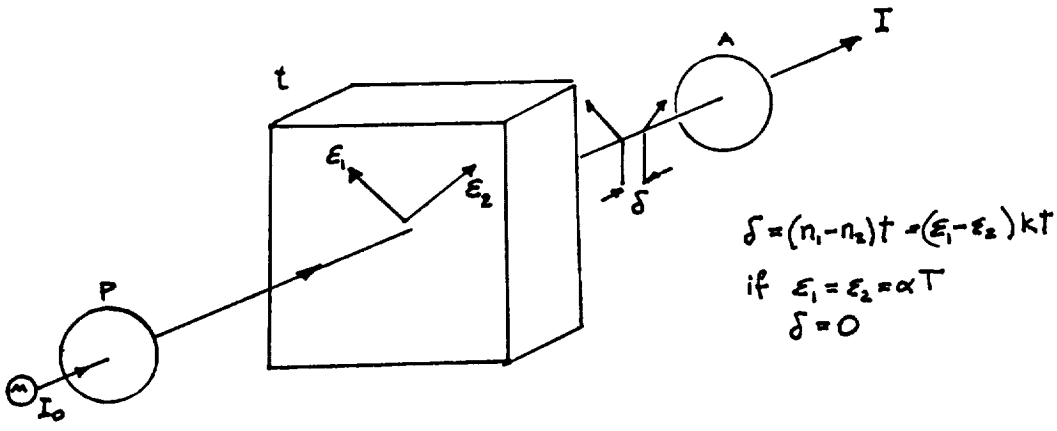

Fig. 1. Temperature Response of Birefringent Sensor

2. PHASE II RESEARCH

2.1 High-Temperature Optical Materials

In Phase I research (1) several transparent materials were considered for possible use. (see Table I). After considering the properties of the available choices, fused silica was selected, since it offered several significant advantages:

- Low cost
- Low index of refraction
- High Brewster constant
- High stability up to 1100° C
- Freedom of initial birefringence

Since in the Phase II higher operational temperatures were implemented, the list of potential candidates was exapanded. Five materials that appeared as good candidates for high-temperature sensing were selected, and their Brewster constant measured at room and elevated temperature, before the final choice was made.

2.1.1 Measurements of Brewster Constant at Elevated Temperature

The calibration of fused silica was performed at room temperature on a ½" x 1" x 6" specimen subjected to uniaxial compression. The Brewster constant was found to be $C = 3.4 \times 10^{-12}$ m^2/N.

The calibration at elevated temperatures was performed in a high-temperature test chamber, on a disc subjected to diametrical compression. The force was carried by a stainless-steel lever system and measured by a load cell placed outside of the oven. (see figure 2)

The fringe order was measured visually using a Senarmont compensator at temperatures ranging from room temperature up to 1100° C.

The photo figures 3 and 4 show the experimental set-up, the specimen installed inside the oven and the lever system used.

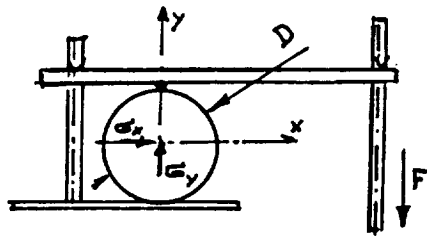

For a disc subjected to a diametrical compression the stresses at the center are:

$$\sigma_1 - \sigma_2 = \frac{8F}{\pi Dt} \qquad (4)$$

and the retardation measured at the center is:

$$\delta = C_B (\sigma_x - \sigma_y) \times t = \frac{8F}{\pi D} C_B \qquad (4a)$$

Fig. 2. Test Set-Up for Measuring C at Elevated Temperature

TABLE I. CANDIDATE OPTICAL SENSOR MATERIALS

Material	Formula	Melting Point	Crystaline Structure	Index of Refraction
Aluminum Nitride	AlN	> 2200	hexagonal	
Sapphire	Al_2O_3	2053	rhombohedral	1.765
	Be_3N_2	2200	cubic	
	CaO	2580	cubic	1.838
	$CaZrO_3$	2550	monoclinic	
	CeO_2	2600	cubic	
Spinel	$MgAl_2O_4$	2135	cubic	1.723
Periclase	MgO	2800	cubic	1.736
Silicon Carbide	SiC	2600	hexagonal or cubic	2.645 2.697
Silica	SiO_2	1800	amorphous	1.456
Zirconia	ZrO_2	2700	monoclinic below 1000 C Cubic above 1000 C	
Zircon	$ZrSiO_4$	2550	tetragonal	1.92-1.96 1.97-2.02

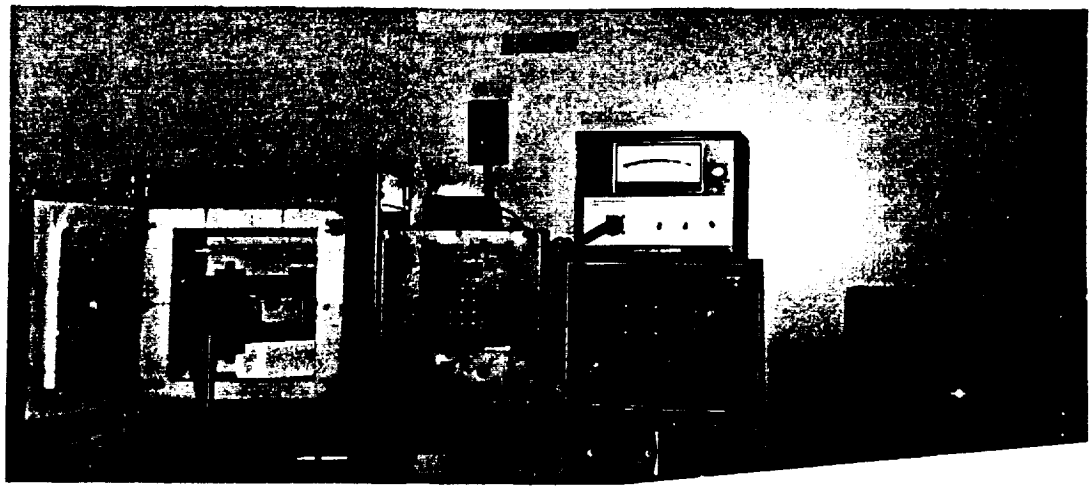

Figure 3 . Experimental Set-Up for Measurements of Birefringence at Elevated Temperatures

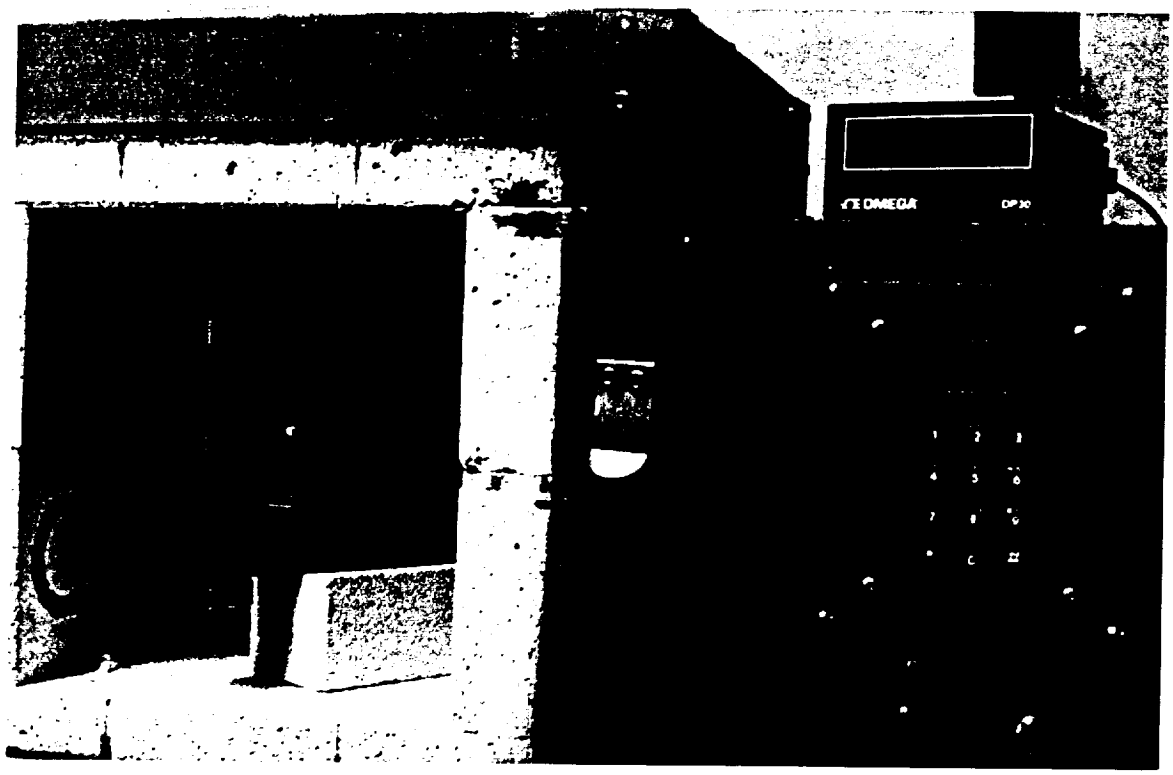

Figure 4 . Fused Silica Disc Subjected to Stress using Dead Weights and Levers.

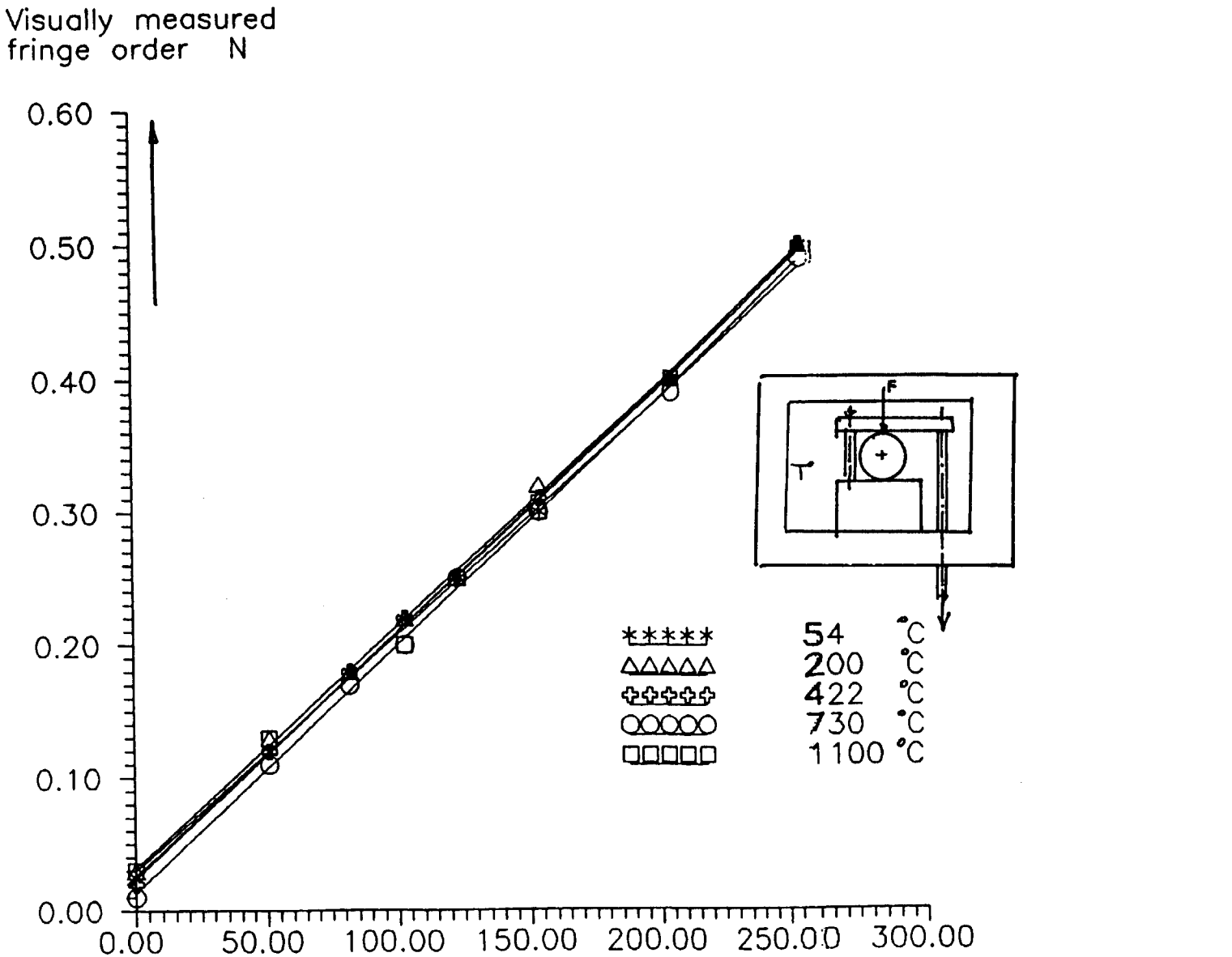

FIG. 5. EVALUATION OF STRESS-OPTIC RESPONSE OF FUSED SILICA VS. TEMPERATURE.

yielding:

$$C_B = \frac{\delta}{F} \frac{\pi D}{8} \qquad (4b)$$

The graph figure 5 shows the measured fringe order N vs. F at various temperature levels. The fringe order was measured using SENARMONT (3) analyzer rotation method, yielding the fringe order N and the measured retardation. The figure 5 clearly demonstrates that:

a. The Brewster constant remains constant between room and 1100° C.

b. The measured birefringence yields the stress and is independent of the temperature.

The materials that were investigated and calibrated are listed below:

MAT'L.	MELTING POINT° C	BIREFRIN-GENCE	BREWSTER CON-STANT 10^{-12}/Pa	ELASTIC MODULUS 10^6 psi	STRENGTH ksi	AVG. INDEX OF REFRAC.	CTE 10^6/°C
Fused Silica	1,800°	None	3.4	10	7	1.46	0.5
Sapphire	2,040°	.008	1.2	50	40	1.75	8.4
Magnesium Fluoride	1,270°	.012	1.7	20	7.6	1.38	13.7
Spinel $MgAl_2O_4$	2,135°	None	1.6	30	15	1.72	7.5
Silicon [Pure]	1,410°	None	20	16	13	3	2.9

Originally, sapphire was considered as the most advantageous choice. Its key advantages are: high-temperature stability combined with hardness, strength, and high-modulus. These advantages are, however, offset by the low Brewster constant, and initial birefringence, combined with a relatively high coefficient of thermal expansion. In our final analysis, the sapphire was therefore rejected, and the design effort was concentrated on fused silica.

SILICON should remain for further consideration, for the design of miniaturized version. (see transducer design below).

Also, SPINEL offers an excellent combination of properties and should be considered as an alternative choice, although its Brewster constant is very low.

The disadvantages of fused silica are:

-Brittleness
-Very low coefficient of thermal expansion and the associated difficulties in designing a seal.

These difficulties were resolved, as described in the "seal design" below.

2.2 Design of the Pressure Sensor

2.2.1 Summary of Phase I Sensor Design

In the Phase I research demonstrating the feasibility of a high-temperature birefringent sensor a simple diaphragm concept, (originally proposed by L. Wesson ( )) was used.

In this concept the light beam travels in the direction parallel to the surface around a disc-shaped diaphragm. The equation relating the retardation δ to the measured pressure P_i was derived in the Phase I research ( ).

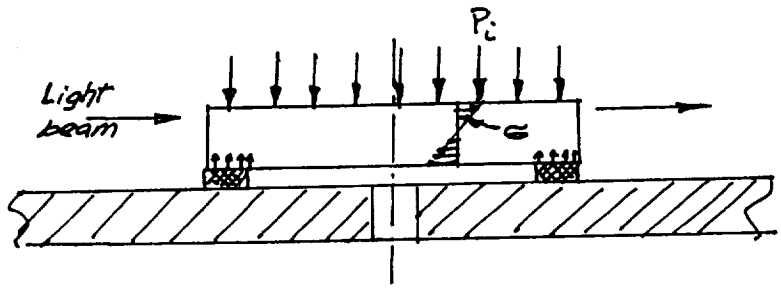

Fig. 6. Diaphragm Photoelastic Pressure-Sensor Concept

This concept is very simple, however, it is potentially offering several problems:

a. In a relatively slender diaphragm, there is a steep gradient of the stress across its thickness, and a relative displacement between the light beam and the sensor introduces a substantial change in output.

b. Clamping forces are located near the sensing area, introducing possible changes in output, as a result of change in clamping forces due to changes in operating temperatures.

2.2.2 Phase II Design Concept

In Phase II, the fundamental diaphragm concept was retained, and the design effort was directed toward elimination of the problems associated with a slender diaphragm, eg.

a. Elimination of thermal stresses from the region where the pressure is measured.

b. Elimination of the gradient in the measured area, in order to minimize the influence of relative displacement due to large variation of temperature, and differences between the CTE of housing and sensor materials.

The basic design geometry is shown in figure 7 . In this geometry several parameters can be modified, to optimize the design. The key features that were investigated included:

Height of the Cylindrical Body - The function of the cylindrical portion was two-fold:

- To test the output of the cylinder as a potentially simple sensor.

- To place the clamping forces far from the measured area, and eliminate their influence on the output.

Rib-On-the-Cylinder Design - This key design concept permitted the elimination of the stress gradient in the area where the light beam crosses the sensor.

Unlike the cylinder or a diaphragm of simple geometry, where the stresses can be predicted analytically, the RIB-ON-THE-CYLINDER geometry cannot be reliably calculated. Using a photoelastic model the RIB design was experimentally evaluated and optimized. This optimization was carried in several steps, investigating the end angle α (see figure 7), and the height H/path T ratio.

Using the photoelastic model-optimation technique, the design was finalized in a very short time, and the final drawings were available in approximately three months after the starting date. (4)

2.23. Photoelastic Model

The sensor geometry defines the stress distribution, stress gradient in the area observed by the beam of light, determines the linearity of response, deflection, speed of response, and the safety margin or overload protection. In fact, every key element of the transducer directly depends on the successful design. For the high-temperature pressure sensor two geometries were retained, for analysis and refinement.

Sensor Geometry A

This geometry is a refinement of a thick diaphragm concept used in the Phase I sensor and is schematically shown in the figure (7).

In this concept the diaphram includes two flats defining the path "t" subjected to a stress σ_θ. The boundaries of the flat section defines the stress gradient. The objective of the photoelastic model analysis was to:

a. Minimize the stress gradient in the region crossed by the light beams.

b. Measure experimentally stress σ_θ at pressure P_i.

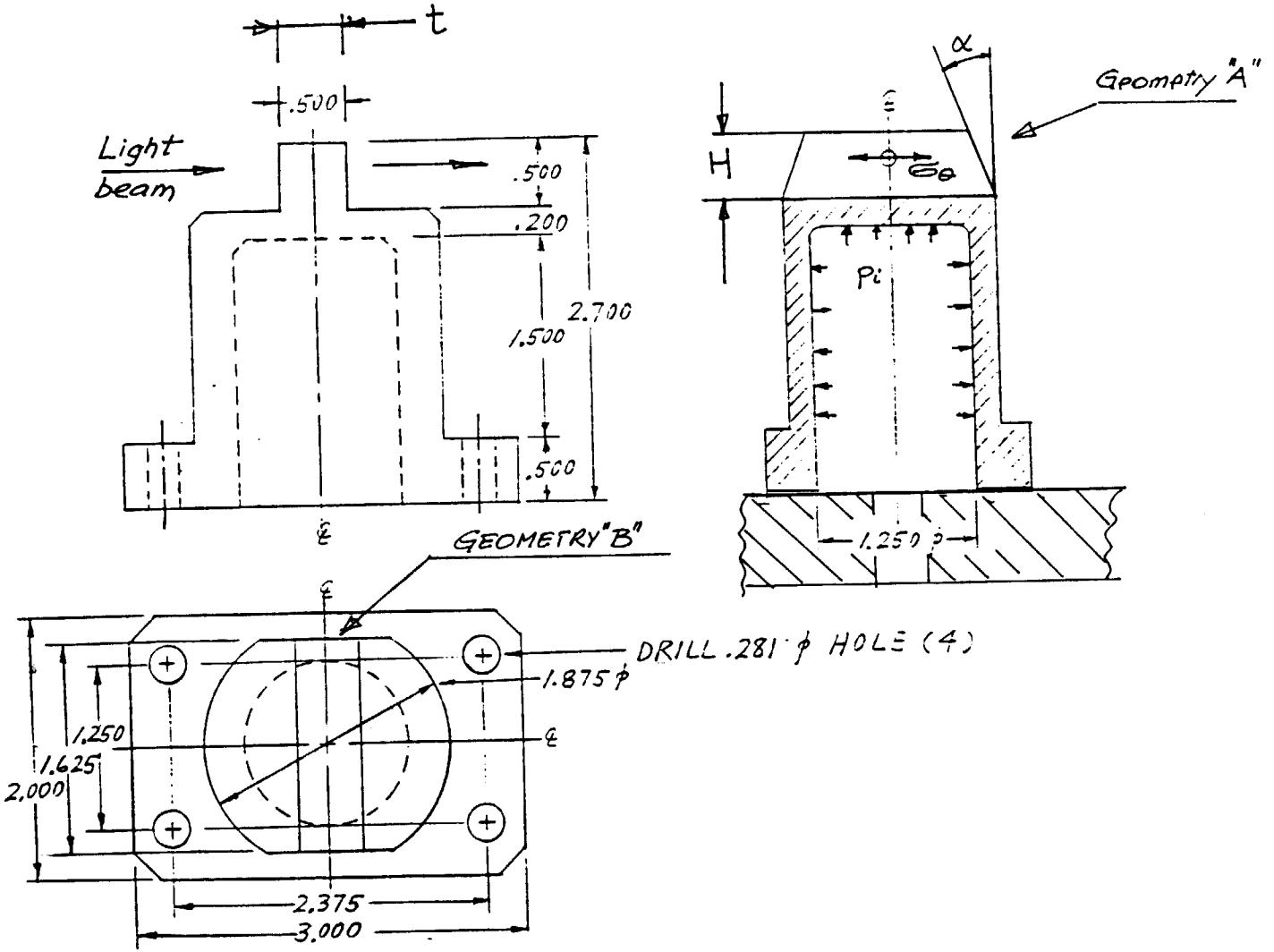

Fig. 7. Sensor Geometry - Dimension of Photoelastic Model

Sensor B

The sensor B geometry was selected for its simplicity and immunity to thermal response. This geometry (see below) is obtained by simply

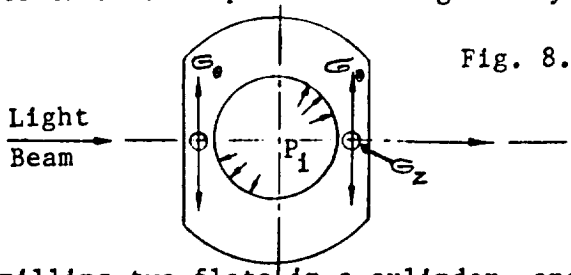

Fig. 8. Modified Cylinder Geometry

milling two flats in a cylinder, and accomplishing a significant local increase of σ_θ without increase of σ_z, enhancing the photoelastic response, $\sigma_\theta - \sigma_z$

In both instances the birefringence and the retardation δ can be expressed by:

$$\delta = C_B \times t \times (\sigma_\theta - \sigma_z) \qquad (5)$$

The model was designed to include the design details of both Models A and B. After an initial evaluation, the model dimensions were analytically calculated to yield stresses necessary to maintain the prototype retardation at approximately 0.3 .

$$I/I_o = \sin^2 \pi\delta/\lambda$$

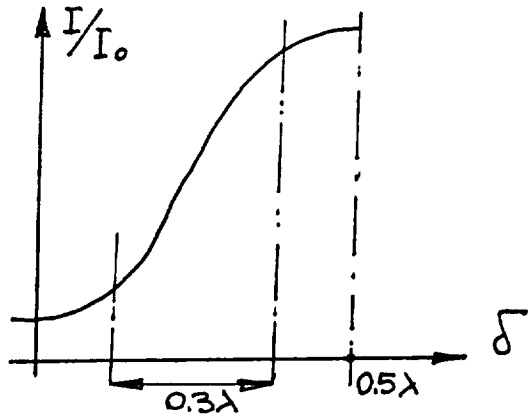

The selection of 0.3λ permits the most effective use of the available span.

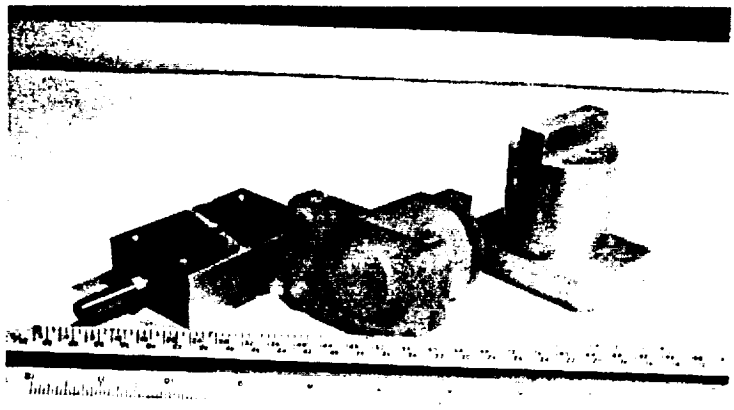

Fig. 9. Photoelastic Model

Construction of the Model

The model was cast using CIBA epoxy resin, cured at room temperature with a tertiary amine hardener. To produce a stress-free model, a slow-cure schedule was adopted, including first a 24 hour slow room-temperature cure, followed by final cure at 200° followed by a 250° F post-cure. (4)

The model was cast to a nearly final shape in a silicon rubber mold. The mold cavity was obtained using a machined-aluminum pattern and a round rubber core, centered to minimize the wall thickness irregularities and avoid shrinkage stress in the curing.

The photo figure 9 illustrates the aluminum pattern, core, and the final casting. After the completion of the cure, the flange and the ID were machined to the final dimensions.

A tensile specimen was cast from the same mix and used to establish the Brewster constant C_B of the model material. The model material was calibrated using a tensile specimen and the Brewster constant was found to be C_B = 52 Brewsters.

2.2.4 Testing of the Model

Three series of tests were designed:

First Series - In the first series of testing, the parameter investigated was the angle α at the top of the rib. Starting with "zero" angle α, the model was tested, recording the fringe order $N = \sigma/\lambda$ vs. pressure at three points, (points #1, 2, 3 see figure 10) to investigate the stress gradient in the area of the light beam crossing. Figure 11 summarizes the results.

Three angles 0°, 30°, and 45° were tested. The model was machined after each test to a new angle and the test repeated.

Second Series - Measurements at the rib were compared to the cylindrical area, and to "flats", (See Figure 8) evaluating the design efficiency for miniaturization parameters.

Third Series - The analysis of results of series 1 and 2 demonstrated that the change of angle α at the rib produced an increase of shear stress at the diaphram-rib interface, while the stress in the region of interest remained lower than the stress in the cylinder. In order to rectify this situation, the height of the rib was reduced from 0.5" to 0.350, and the test repeated, collecting the data in all regions. Figure 11 shows the results obtained. Figure 12 shows the photoelastic model subjected to internal pressure, installed in a polarimeter PS-100 for measurement of fringe order N.

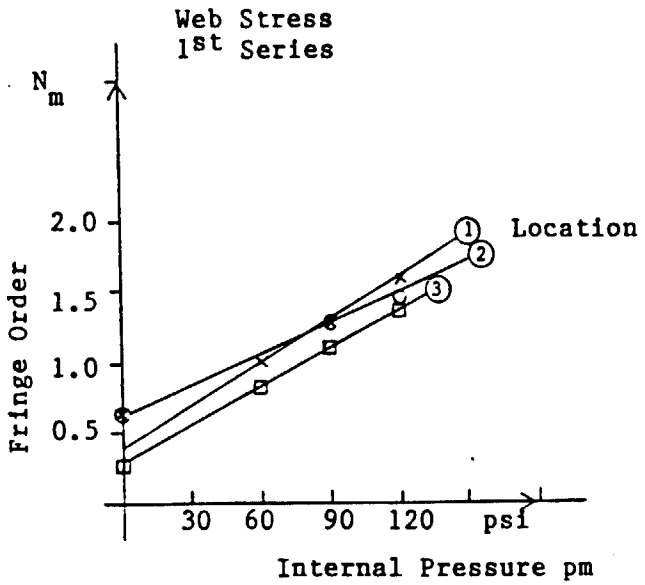

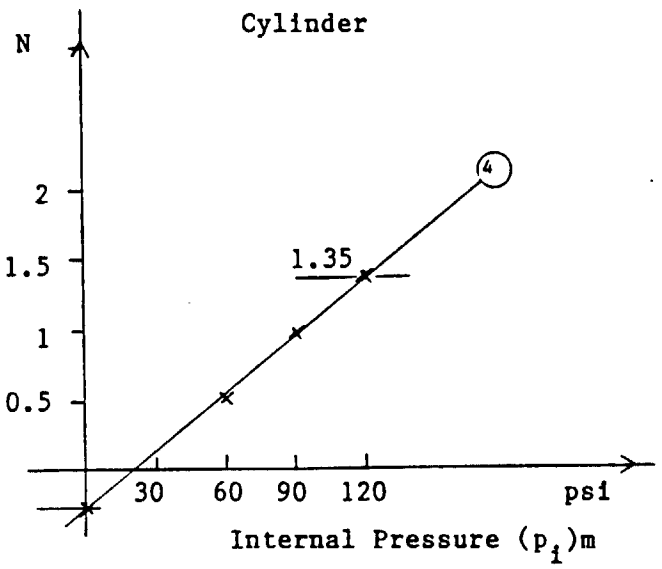

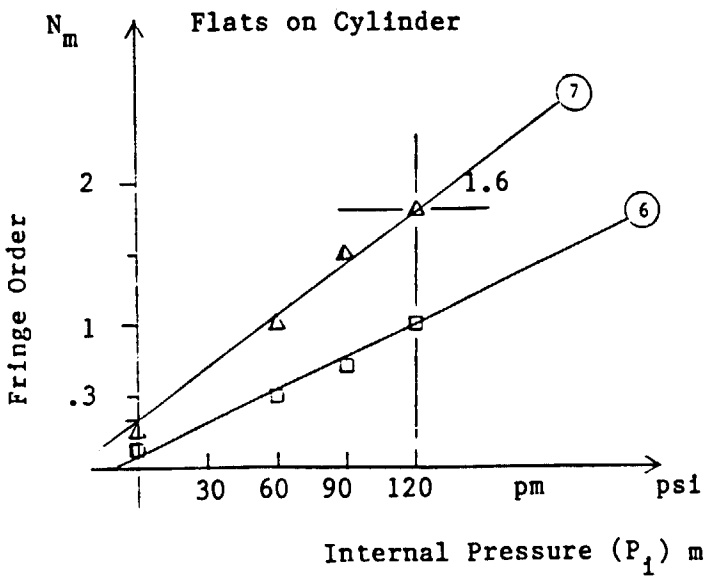

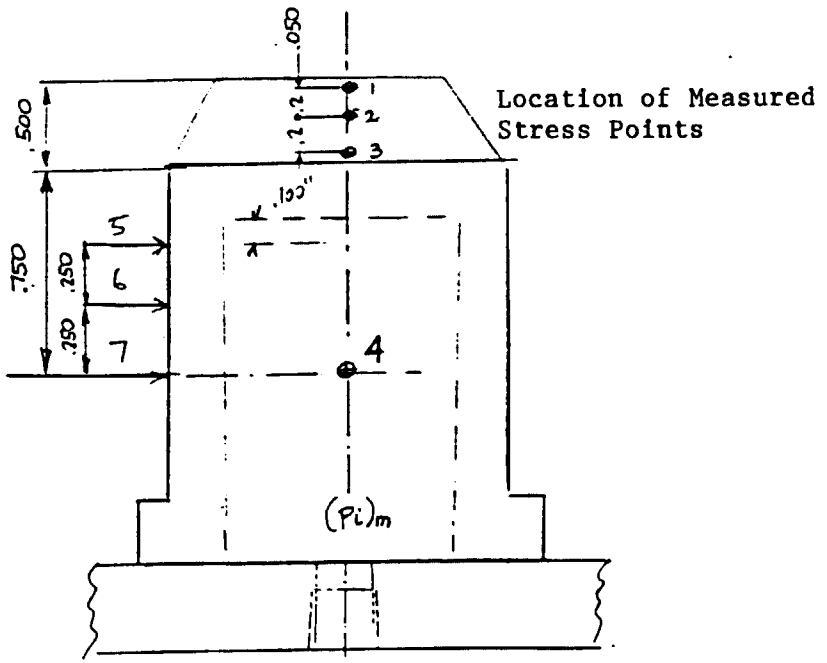

Fig. 10. First Series of Model Testing. Optimation of Angle α.

First Series - Optimation of Angle

TABLE I

Pressure psi	$\alpha = 0$ Point #			$\alpha = 30°$ Point #			$\alpha = 45°$ Point #		
	1	2	3	1	2	3	1	2	3
0	0	0	0	0	0	0	0	0	0
60	.50	.42	.56	.54	.58	.63	.51	.60	.74
120	1.07	.98	1.10	1.10	1.09	1.14	1.07	1.26	1.46

Second Series - Optimation of Output

TABLE II

Comparison of Output between Configurations "A" and "B"

Point #	0	60	90	120	LOCATION
1	.6	1.0	1.3	1.60	web
2	.6	1.0	1.3	1.45	"
3	.25	.83	1.1	1.46	"
4	-.25	.50	1.0	1.35	cylinder
6	+.1	.5	.70	1.0	flat
7	+.26	1.04	1.50	1.78	flat

TABLE III

Optimation of H/T Parameter. Reduced Rib-Height

Test Configuration #4, Reduced web .35" high

Point #	0	30	60	90	120 psi.
1					
2	.10	.5	.90	1.30	1.75
3	.25	.5	.85	1.15	1.55
4 (cylinder)	-.21	.17	.52	1.0	1.40
6	.1	.3	.5	.70	1.1
7	.33	.65	1.1	1.25	1.75

Fig. 11. Results of the Photoelastic Model Test

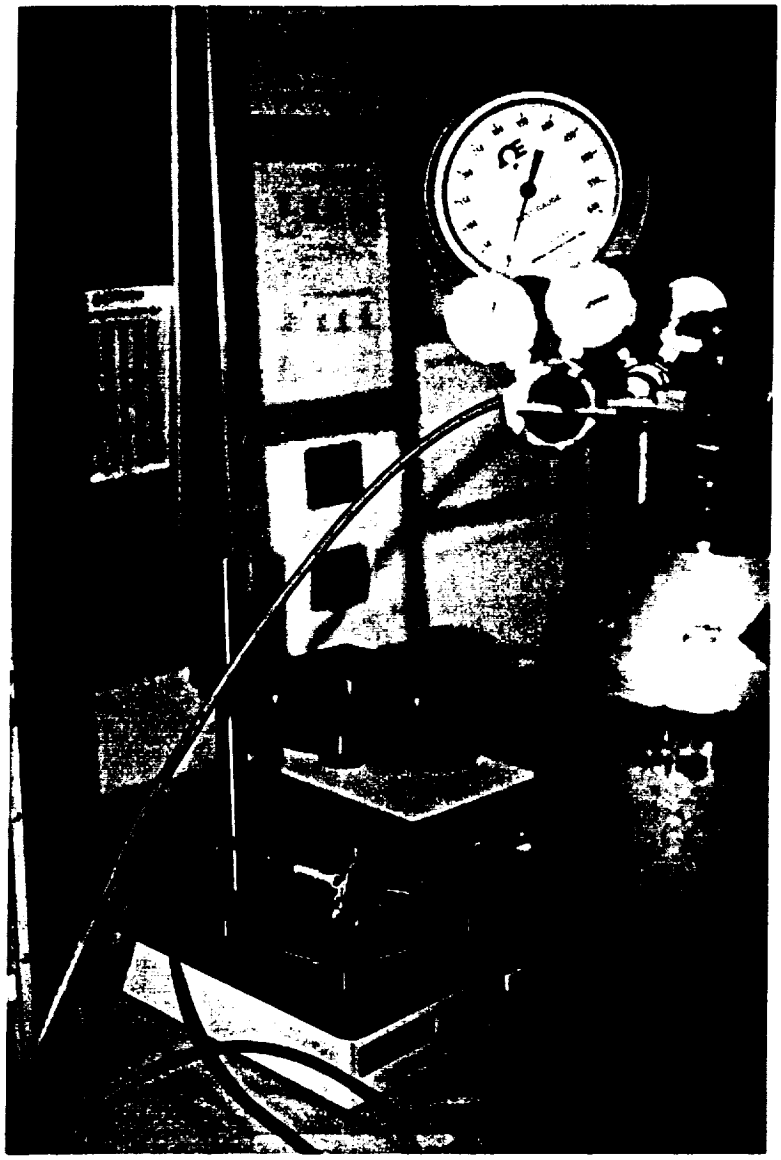

Fig. 12. Testing of Photoelastic Model Subject to Internal Pressure Using SA-100 Polarimeter

The series 3 produced satisfactory design and the desired results. From all the tests, the following conclusions were drawn:

1. The design using "flats" on a cylinder is considered impractical, since as a result of the thickness changes, the stress is non-uniform, making the location of the beam very critical.

2. The use of a purely cylindrical geometry appears to be useful and advantageous. This concept should be retained for the future, but it will require a reflection technique and careful selection of a combination of spherical and cylindrical lenses.

3. The rib-on-the-cylinder concept was selected for the final geometry. The drawing (Figure 13) shows the final dimensions, taking into consideration the scale factor and wavelength consideration.

2.2.5. Scale Factor

In order to translate the results of the model testing into actual sensor dimensions, the following relations apply: (4)

Subscript m model
Subscript P prototype sensor

$\frac{L_m}{L_p}$, $\frac{\delta_m}{\delta_p}$, $\frac{\lambda_m}{\lambda_p}$, $\frac{P_m}{P_p}$, $\frac{C_{Bm}}{C_{Bp}}$, $\frac{\sigma_m}{\sigma_p}$, are dimensionless scale factors respectively of length L, retardation δ, wavelength λ, pressure P, Brewster constant C_B, and stress σ. From the dimensional analysis it follows that:

$$\frac{\delta_m}{\delta_p} = \frac{C_m}{C_p} \times \frac{t_m}{t_p} \times \frac{\sigma_m}{\sigma_p}$$

Since the retardation $\delta = N\lambda$ (N is the measured fringe order), it follows that:

$$\frac{\delta_m}{\delta_p} = \frac{N_m}{N_p} \times \frac{\lambda_m}{\lambda_p}$$

Using a wavelength of 570 nm in the model analysis and 830 nm in the sensor measurements, $\lambda m/\lambda p = 570/830$.

In order to remain in the normal operating range, the maximum fringe order Np desired in the sensor is approximately 0.3.

The fringe order Nm measured in the photoelastic model at 120 psi pm (see table of results, series 3).

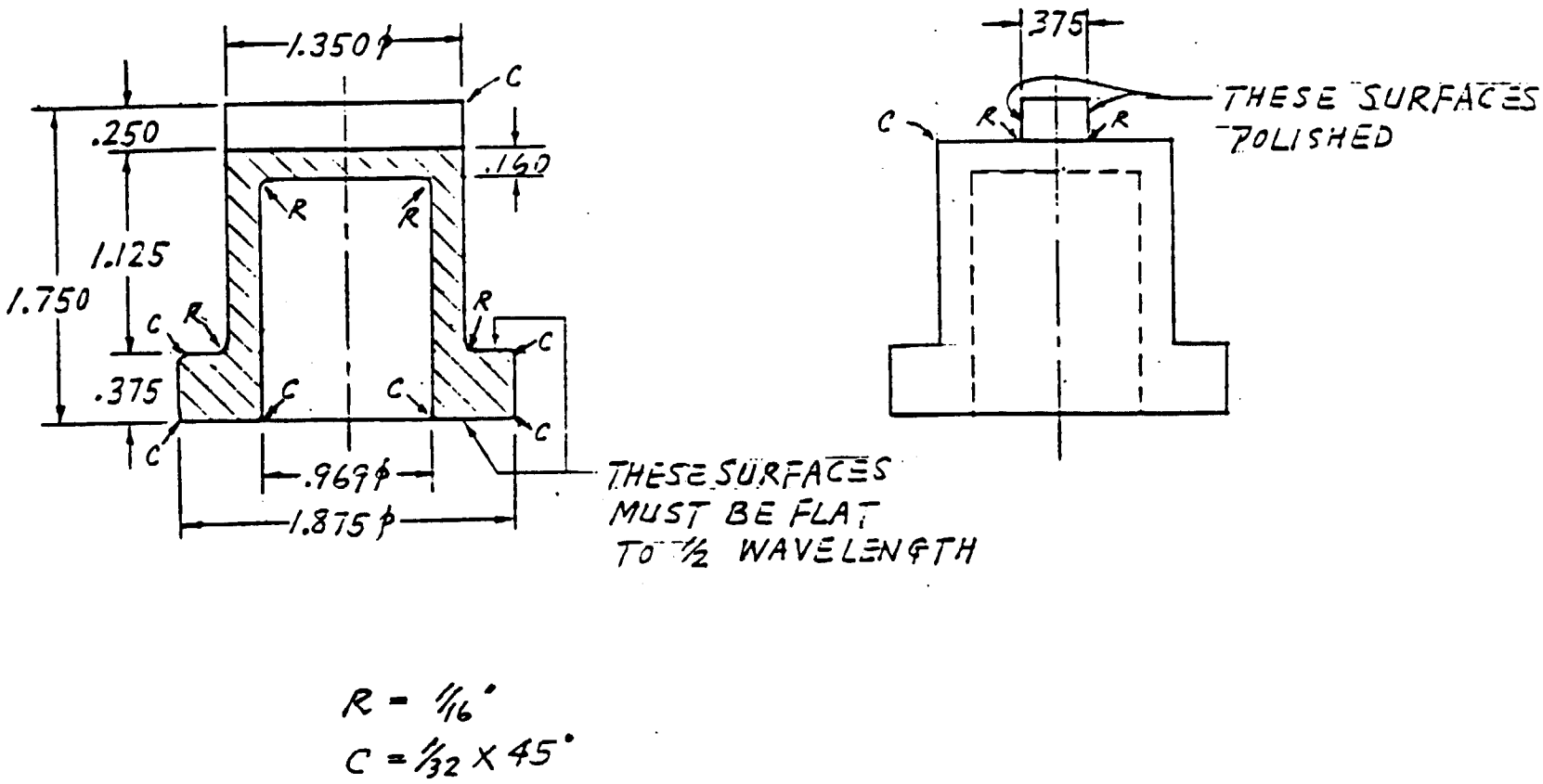

Fig. 13. Final Sensor Geometry Derived from Photoelastic Model Test

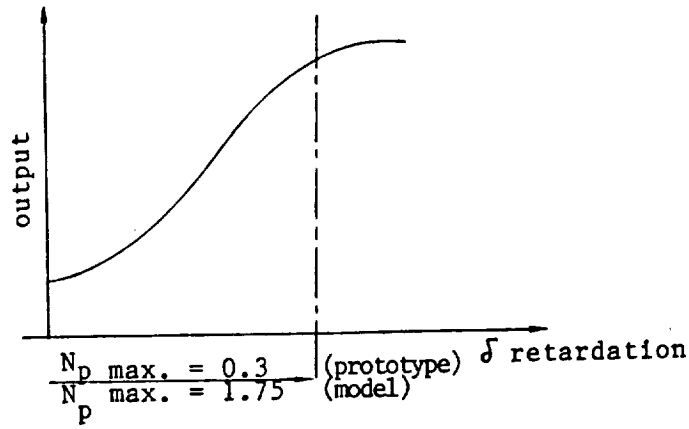

In order to obtain Np = 0.3 at 500 psi sensor pressure, the length scale becomes:

$$\frac{l_m}{l_p} = \frac{\delta_m}{\delta_p} \times \frac{C_p}{C_m} \times \frac{P_p}{P_m} = \frac{N_m}{N_p} \times \frac{\lambda_m}{\lambda_p} \times \frac{C_p}{C_m} \times \frac{P_p}{P_m} \qquad (6)$$

Substitution of the actual scale factors yields the final length scale:

$$\frac{lm}{lp} = \frac{1.75}{0.3} \times \frac{570}{830} \times \frac{3.4}{52} \times \frac{600}{120} = 1.31$$

The sensor prototype dimensions were obtained dividing the model dimensions by 1.31 and rounding-up to the desired final dimensions.

2.2.6 Miniaturization of Design

In the final design effort, additional consideration was given to weight, physical dimension, and ability of the transducer to perform in a force field (acceleration).

The original sensor design (see drawing Figure #7) proposed two geometries: one based on the cylindrical wall sensing, the other one on the "Rib-on the Top of a Cylirder" design. The output stress in a pressure vessel can be expressed as:

$$\sigma = \frac{pd \cdot K}{2t}$$

The photoelastic output is then computed from the stress, the light path, and Brewster constant:

$$\delta = \sigma \times \text{path} \times C_B \qquad (8)$$

Using a straight cylindrical path, one obtains:

$$\sigma = 0.25 \frac{pd}{t} \text{ and path} = 2t$$

from above:

$$\delta = 0.5\ pd\ \times C_B \tag{9}$$

While the analytical expression of stress in the "Rib-on-the-Top" design is not available, our experimental results demonstrated that the output (see Figure 11) is about the same or slightly higher than predicted by the equation above.

From the above, it can be established that the MINIMUM diameter of the PHOTOELASTIC PRESSURE SENSOR is given by:

$$d\ \text{min} = \frac{2\ \delta \text{min}}{p\ C_B} \tag{10}$$

One must also insure that the stresses remain below the strength of material requirement, in particular:

$$\sigma < \frac{pd}{4t} \tag{11}$$

For 500 psi (3.45 MPa) pressure and 0.3λ retardation (δ= 246 nm), the above equations yield (for cylindrical sections and fused silica material).

$$d\ \text{min} = \frac{2 \times 246 \times 10^{-9}}{3.45 \times 10^{6} \times 3.4 \times 10^{-12}} = 47 \times 10^{-3}\ \text{m} = 1.65\ \text{in.} \tag{12}$$

As a result of the web-optimation photoelastic work, we have succeeded to improve the "shape" factor and produce a sensor that is smaller (d = 1.35 in.) than the theoretical.

Further mainimization of the transducer can be accomplished only by replacing the fused silica sensor by another material, exhibiting larger C_B . An additional potential candidate for a birefringent transducer material is Silicon. While its melting point (1410° C) is considerably lower than the melting point of the fused silica (1800° C) the Brewster constant (C_B = 20 Brewster) is considerably higher. Using similar analysis (see equation above) the minimum cylinder diameter becomes:

$$d\ \text{min} = \frac{2 \times 0.3\lambda}{p \times C_B} = \frac{2 \times 0.3. \times 10^{-6}\text{m}}{3.45\ \text{Mpa} \times 20 \times 10^{-12}/\text{Mpa}} = 8.7 \times 10^{-3}\ \text{m} = 0.34\ \text{in.}$$

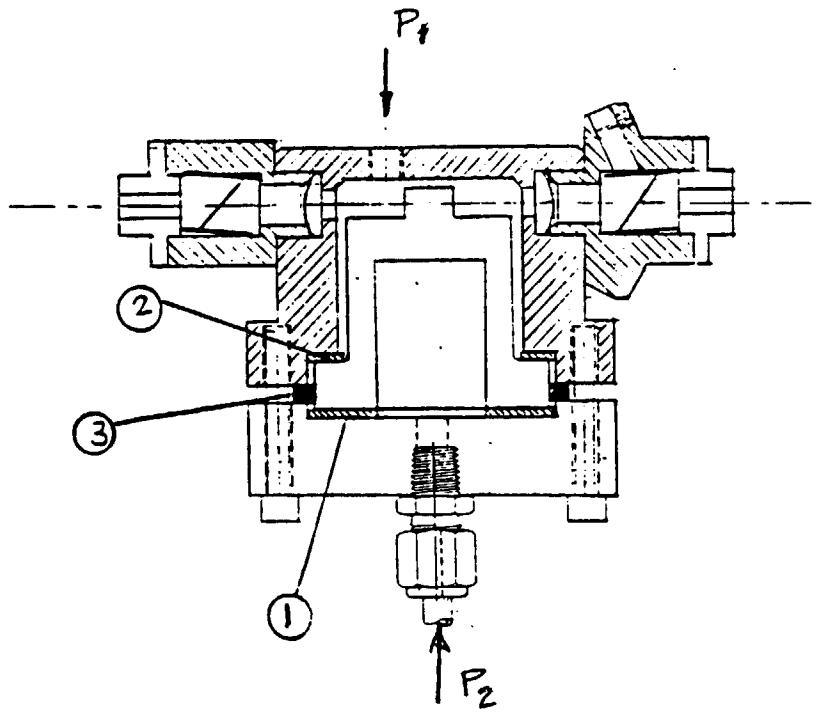

FIGURE 14. Fused Silica Sealed and Mounted in its Transducer Housing

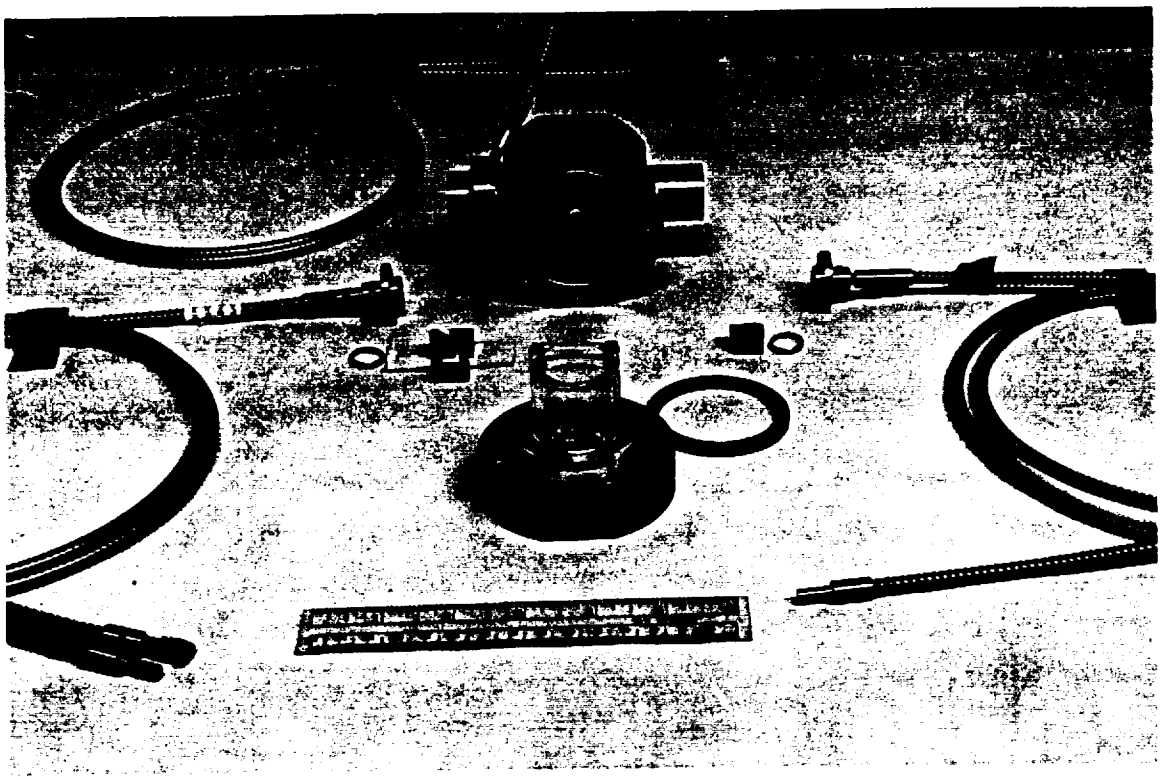

Fig. 15. Completed Transducer - 1st Version - for Testing at 600° C.

Fig. 16. Set-Up for System Testing at 600° C.

The above analysis suggests that the fused silica sensor is already minimized and optimized to its minimum dimension, and only a change in sensor material to semiconductor-grade silicon can substantially reduce further the overall size. Such a change would, however, reduce the temperature capabilities to approximately 1000° C.

In Phase III of this project, a silicon transducer should be considered, since it will be the most suitable choice for a commercial application, whereby the 1000° C capability appears sufficient.

2.2.7. Housing Design and Seals

Two prototypes were designed and tested. In the first prototype, (see figure 14), a greater degree of flexibility was incorporated, to permit comparative mertis of several seal pressure configuration. (see figure 15)

This design, although bulky and complicated, allowed testing using ports p_1 and p_2 subjecting the sensor to tension or compression, and allowed for test and evaluation of merit of different seal locations (1,2, and 3 see figure 14).

As expected, it was found that the use of the pressure port p (placing the flange seal #1 and also the sensor body in compression) insures a better seal. This choice (also adopted in the Phase I) introduces an additional burden, since the seal of the optical path must be separately insured.

The design of the polarizer holders and fiber-optic cable connection was determined by the selection of these components (see 2.2 and 2.3 above).

The most serious difficulties were experienced with the polarizer crystals. (GLAN-LASER)

The experience gained with the first prototype permitted the re-design of the housing and production of the final housing for testing with 1500° C gas temperature.

The final design succeeded by cutting the original design weight in half, and incorporated a multi-material seal design, designed to minimize differences in thermal expansion. Figure 19 shows the cross-section of the final design and a photo of the final transducer housing.

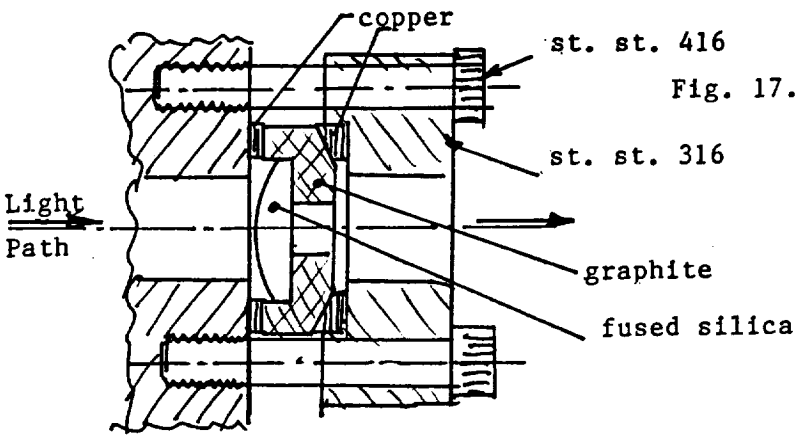

Fig. 17. Seals for Optical Port

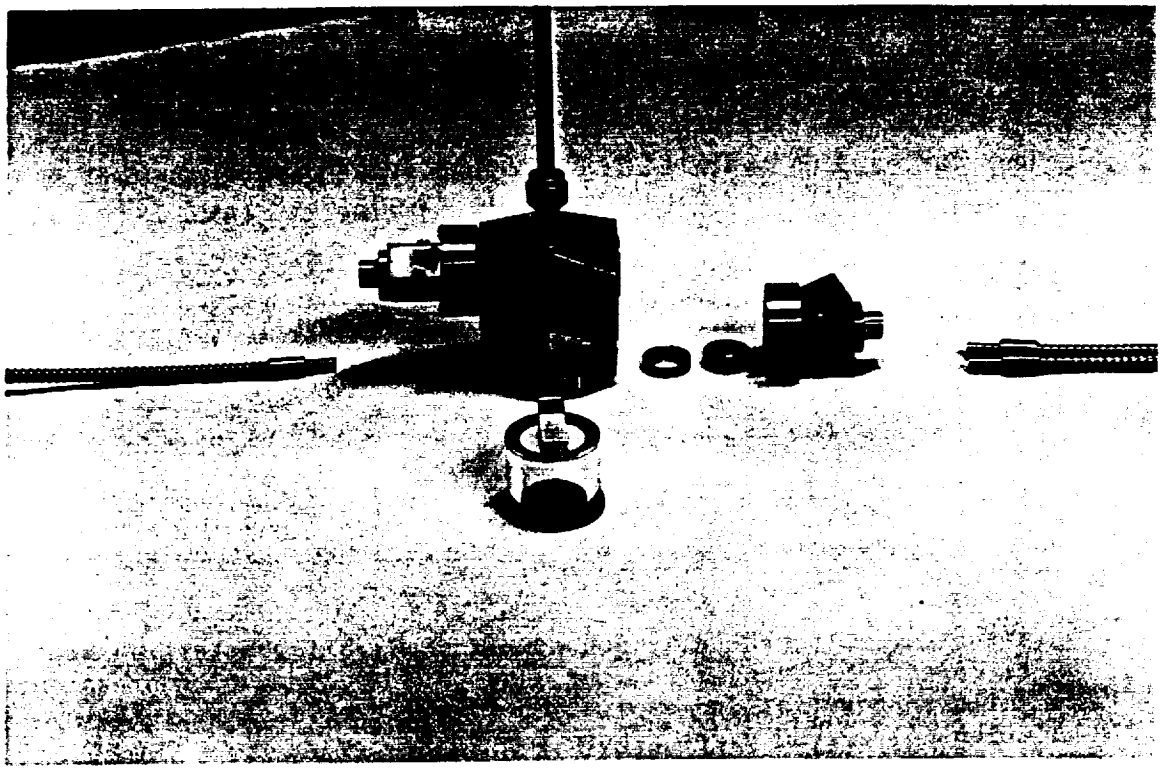

Fig. 18. Photo of Final Transducer Design

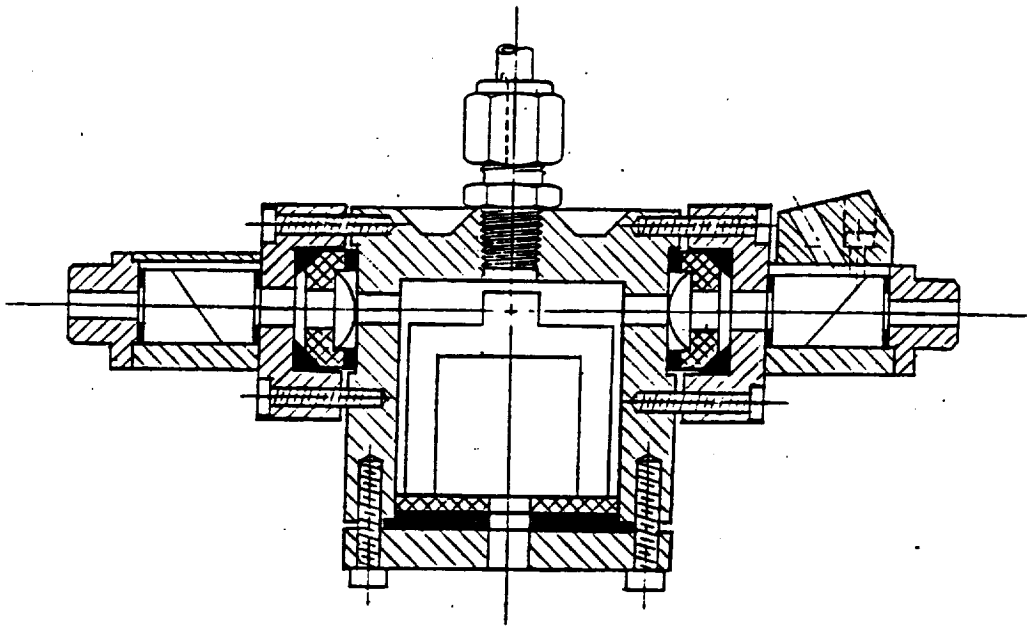

Fig. 19. (Schematic) Final Transducer Design. Final Housing Geometry including Seals of Optical Ports for Testing at 1500° C Gas-Pressure Temperature.

The length dimension of graphite lens-seat, copper gasket and stainless 316 back-up plate were calculated to match the expansion of the bolts SS 416 and maintain the seal force at all temperatures below allowable stress levels.

Unlike the first prototype, the second prototype included an adjustable position of the parallel output. This requirement complicated the housing, but was required as a result of the unpredictable dimensions of crystal polarizers and their tilt requirements. (Figure 20 below)

The port-pressure inlet was connected to high-temperature gas pressuring using SS316 fittings.

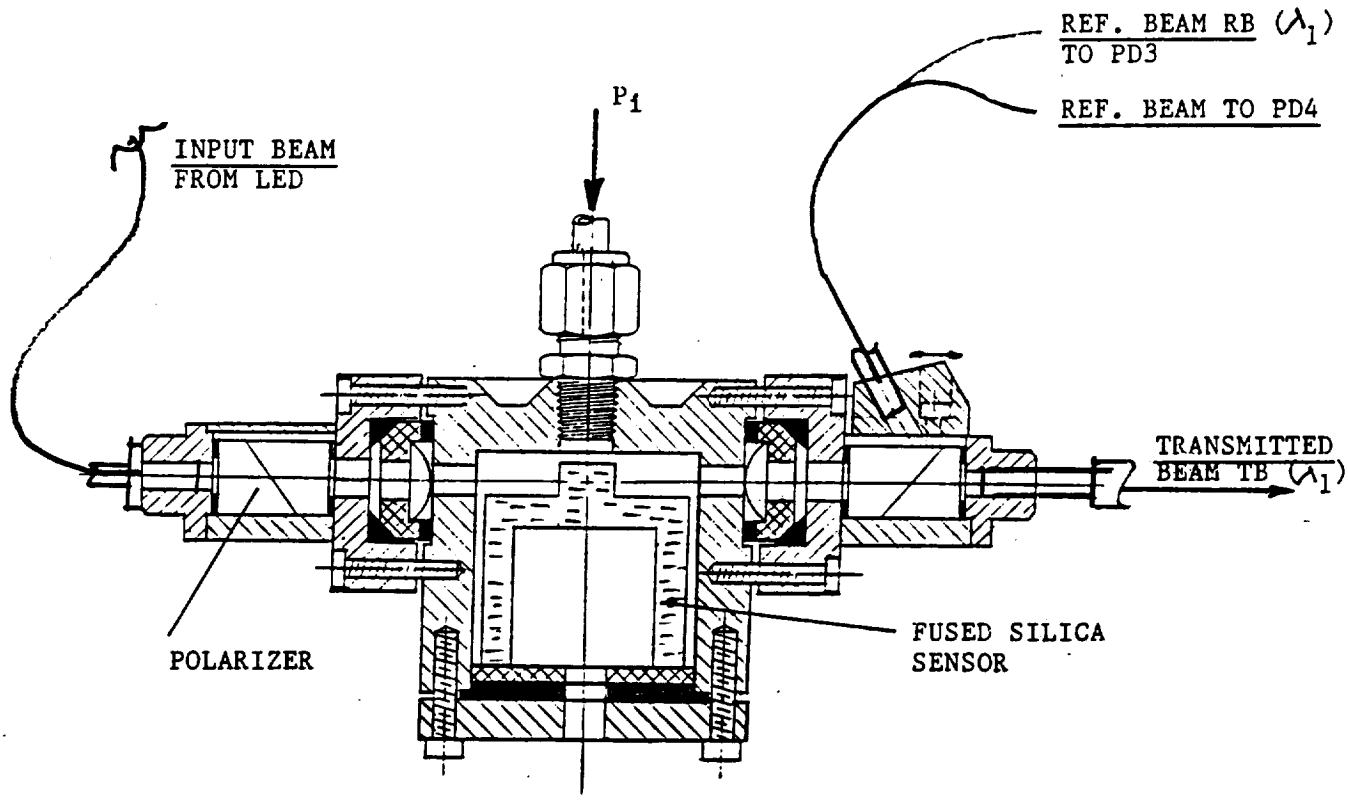

Fig. 20. Detail of Output Cable Attachment

2.3. Polarization of Light at elevated Temperature

An extrinsic birefringent sensor can be operated using any one of the schemes below:

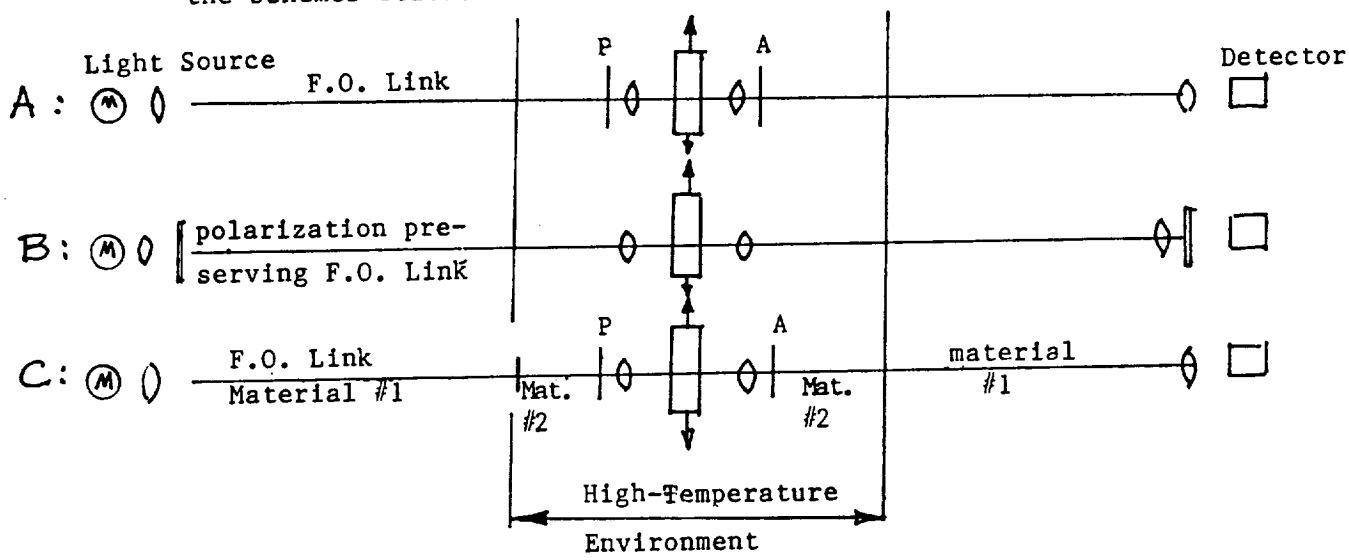

Figure 21. Light Path in a Birefringent Sensor

The schematic B above appears as the most desirable solution, since it places the polarizer P and analyzer A elements near the light source and readout rather than in the hostile environment of the engine compartment. This solution should be retained for future consideration, if and when the polarization-preserving F.O. cable, capable of functioning at elevated temperatures of 600° C required in this project, becomes available.

Presently available polarization-preserving fibers are single-mode, with core diameters of approximately 5 microns, requiring a laboratory-environment coupling to the light source and not rated for operation at elevated temperature. None of the potential suppliers offered an estimate on future availability of elevated temperature capable polarization-preserving fibers.

In Phase I research, schematic "C" above was used, incorporating two separate links "material 1" carrying the signal through a "room-temperature" path, and a "material 2" (approximately 10" long fused silica rod) carrying the light through the high-temperature environment.

In Phase II the full length of the cable was capable of 600° C performance (schematic "A"). (5)

The selection of the polarization means required experimental verification. In the Phase I research (see report Phase I) a complete review of the available means was incorporated.

The multilayer dielectric-coated and dichroic polarizers were rejected because of their inherent temperature limitations. The Brewster-angle concept was selected as most promising, and the "STACK OF PLATES" utilizing multiple Brewster-angle plates was evaluated analytically.

This theoretical evaluation suggested that a stack of plates would provide the expected performance.

THEORETICAL EFFICIENCY OF STACK-OF-PLATES POLARIZER

Plate #	Surface #	Cum. Power in Reflected Polarized Beam % of Input	dB
1	1	6.38	-11.95
	2	11.94	- 9.23
2	3	16.80	- 7.75
	4	21.04	- 6.77
3	5	24.74	- 6.07
	6	27.97	- 5.53
4	7	30.78	- 5.12
	8	33.24	- 4.78
5	9	35.38	- 4.51
	10	37.25	- 4.29
6	11	38.88	- 4.10
	12	40.30	- 3.95
7	13	41.54	- 3.82
	14	42.62	- 3.70
8	15	43.57	- 3.61
	16	44.40	- 3.53
9	17	45.12	- 3.46
	18	45.75	- 3.40
10	19	46.30	- 3.34
	20	46.78	- 3.30

The above calculation does not account for absorption losses and some mutliple internal reflections.

Since the polarization due to Brewster angle could be affected by the actual surface conditions, and the analytical considerations do not take properly into consideration the multiple-reflections occuring and their secondary path, it was decided to run an experimental evaluation of the efficiency.

An example of a possible design that would implement the concept of a high-temperature polarizer, utilizing a "stack of plates" concept is shown below:

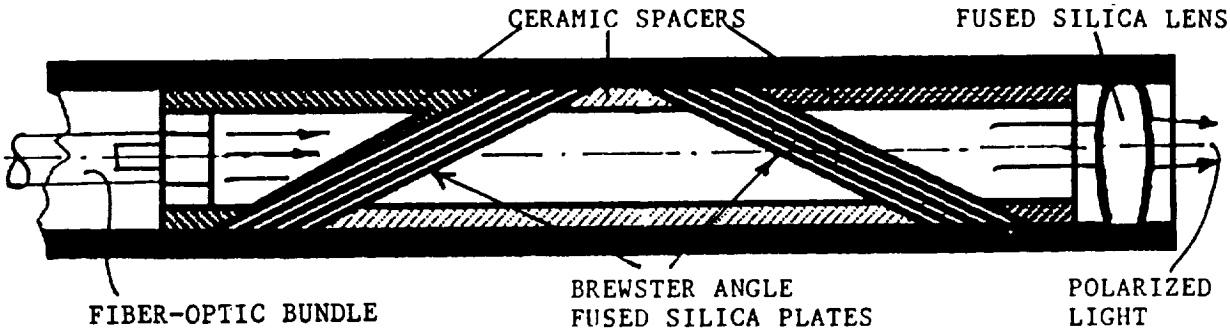

Figure 22. "STACK OF PLATES" HIGH-TEMPERATURE POLARIZER

The symmetric design permits the elimination of the beam deviation. The set-up used for experimental evaluation is shown schematically below.

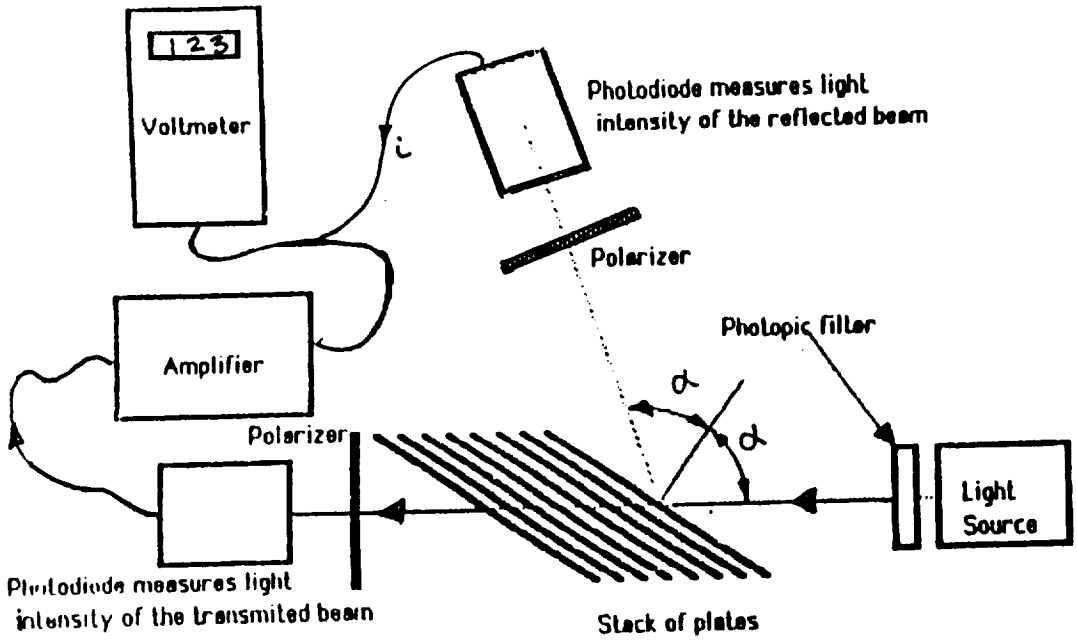

FIGURE 23. Set-Up used for Evaluation of Efficiency of "Stack of Plates" Polarizer.

The results of measurement are shown in the table below. Experiments were carried out for one plate, stack of 4, 6, and 10 plates.

		POLARIZATION EFFICIENCY %	ENERGY EFFICIENCY %
1 Plate	Transmission	23%	9.10%
	Reflection	96.30%	6%
4 Plates	Transmission	57%	14.50%
	Reflection	99.20%	15%
6 Plates	Transmission	68.40%	19.30%
	Reflection	99.1%	16.50%
10 plates	Transmission	83.80%	23%
		99.30%	20.60%

The results were rather discouraging. In the reflection mode a very good polarization efficiency can be obtained, however, it is accomplished with a very poor energy efficiency, by far below the theoretical predictions.

The transmission mode provides a better energy efficiency, however, the polarization efficiency (83.8%) is not sufficient to justify the use of this concept in a transducer.

Since our Phase I expectations were not fulfilled, another approach was investigated and implemented in the Phase II program: A GLAN-LASER PRISM POLARIZER (GLPP). Several suppliers offer an essentially identical product, available in various sizes. The concept utilizes a strongly birefringent material (CALCITE) cube, cut at an angle that generates a critical-angle total reflection for "O" ray, but transmits the "E" ray.

Calcite is an anisotripic, uniaxial crystal which exhibits birefringence. Since the refractive index for the extraordinary ray is less than that for the ordinary ray the material is considered optically negative.

Calcite has a wide range of optical transmission with an absorption coefficient for both the E-ray and O-ray of less than 0.1 from 260.0 nm to 1.7μ. The O-ray has a somewhat greater transmission range (especially in the infrared), but as the O-ray is typically the rejected ray in a calcite polarizer this greater transmission range is not advantageous. the dichroic nature of the transmission is a further result of the anisotropic nature of the material.

Calcite crystals may be formed into very efficient polarizers by causing the ordinary and extraordinary rays to confront an angle within the material that exceeds the critical angle for one of the rays, but not for the other. In this way one of the polarizations is completely separated from the other by total internal reflection. Many forms of calcite polarizer have been designed,but in practice only three, the Glan-Thompson, Glan-Taylor and the Wollaston, styles are of great benefit, and all are similar, the differences between theses styles tend to trade the interdependent relationships between power handling, useful acceptance angle, and beam separation.

Both Glan-type prisms have been designed such that both the entrance and exit faces are normal to the intended direction of use and the prism angle has been cut such that the O-ray is totally internally reflected at the first face. In the case of the Glan-Thompson prism, the two halves are cemented together with an optical cement. In the case of the Glan-Taylor prism, the two halves of the polarizer are separated by an air-space. While the air-space separation does allow the prism to handle substantially higher power levels than the cemented prisms, the useful angular field is reduced.

Whatever form of Glan polarizer is chosen, the prism angle should be selected such that it lies mid-range within the boundaries of acceptable polarizing angles. One side is bound by the angle at which total internal reflection occurs for both the O- and the E-ray; the other is bound by the angle at which transmission begins for both rays. This angle can be optimized only for one wavelength in any particular polarizer and will vary depending on the type of polarizer and whether or not the prism is cemented or air-spaced. In general terms, the acceptance angle for a Glan-Taylor polarizer is typically 8.5° and for a Glan-Thompson prism is 18.5°, as calculated from the theoretical values of the index n_e and n_o.
Typical specifications of Glan-laser linear polarizers are:

Substrate Material: Calcite
Wavefront distortion: $\lambda/4$
Extinction Ratio: 10^5:1
Transmission Efficiency: T 96%
Air spaced for high-power application

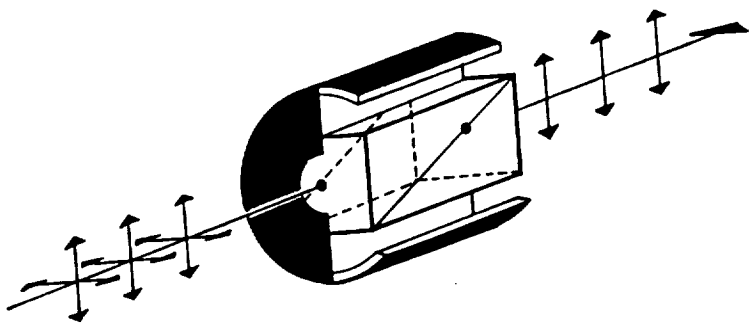

Figure 24. Calcite Prism Polarizer

Polishing the upper face, both E- and O- polarized rays can be retrieved, permitting to obtain the output using "crossed" and "parallel" polarizer and analyzer arrangements,using only one exit prism.

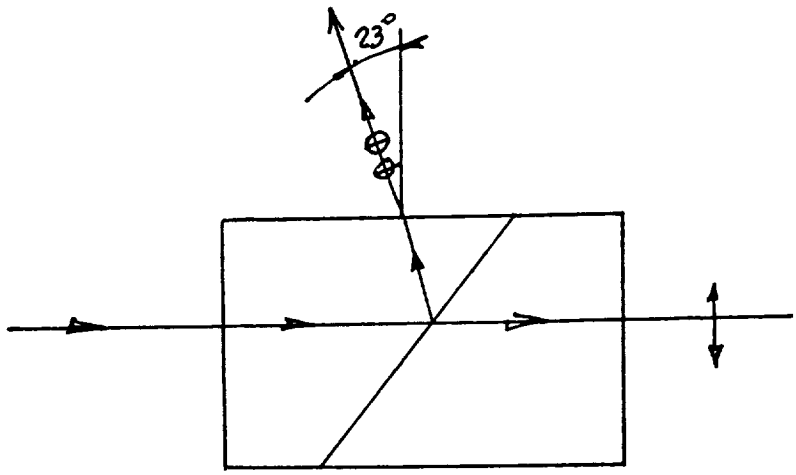

Figure 25. Prism Polarizer providing Exit for "E" and "O" Rays

One of the manufacturers suggested that since some of the coatings are applied to CALCITE at 700° C, this temperature can be safely considered as an operating temperature. Since our objective was to maintain the housing at the engine compartment temperature and test up to 600° C, the CALCITE Glan-Laser polarizer was selected and the transducer design was based on this selection.

Calcite Glan-laser prism (with one-escape window) unmounted, air-spaced were ordered from Karl Lambrecht Company in Chicago, Illinois.

A preliminary test of these prisms revealed that the acceptance-angle was considerably lower than suggested in suppliers' catalogs, and the cut-angle was such that the acceptance angle was unsymmetrical, approximately 6° on one side and 0° on the other side

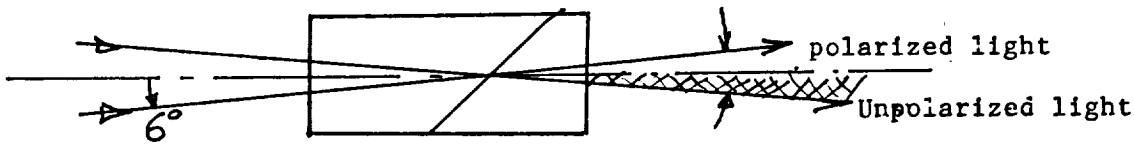

Figure 26. Measured Acceptance Angle

In order to remedy this situation, the prism was positioned at an angle 3° to the incident beam. Using this arrangement, we were able to improve the polarization, but the efficiency was greatly dependent on the NA of the beam crossing the prism, and the high-efficiency expected originally was not obtained.

After the original set deteriorated as a result of extensive testing at 600° C, a new set was procured from Zeta International Company, Prospect, Illinois. The results of the first and second test were the same, revealing an even greater departure from summetry, and a 6° acceptance angle.

As a result of the need to incline the polarizing prism, the design of the prism housing was changed, to permit the aligning of the exit-fiber with the reference output beam. Drawing figure 26 illustrates this detail.

2.4. Fiber-Optic Links

In an extrinsic sensor arrangment used in this project, the fiber-optic link is used for transmission only. The transmitted signal is chopped (see "Readout System" below), but an analogue quantity (amplitude) is measured.

The desirability of a polarization-preserving quality of the fiber was discussed in "Polarization of Light" above. If and when a high-temperature capable polarization-preserving fiber becomes available, it would then become a good choice.

Presently available polarization-preserving fibers are single mode, 5 to 10 microns in diameter. Using such a small diameter in an extrinsic sensor would be highly impractical, since the relative displacement of the input and output mounts due to stress, temperature expansion, and temperature differential would have a very significant influence on the attenuation.

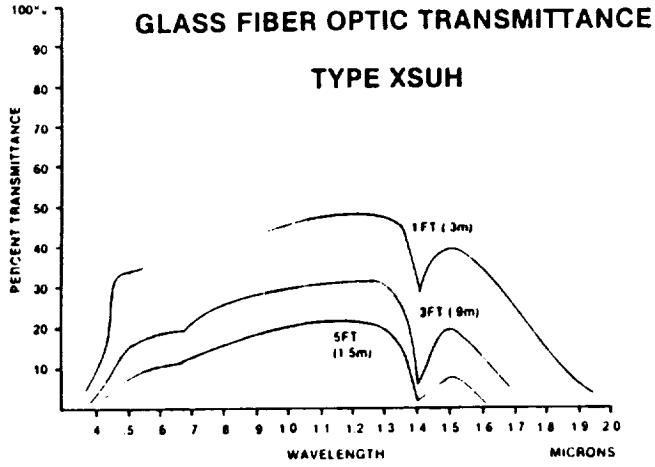

Figure 27. Fiber Transmittance vs. Wavelength

Multi-mode Fibers

Use of large diameter multi-mode fibers and/or bundles eliminates difficulties associated with the single-mode fibers and the sensitivity to the relative displacement is greatly reduced.

The cable assembly selected for use was Dolan-Jenner type XSUH rated for continous operation at temperatures up to 650° C, randomized. These cables are jacketed with an interlocking stainless-steel hose as protective sheathing. The transmittance of the XSUH cable is shown in the figure 27 above. (5)

The individual fibers in the budle are .002 inches (50 microns) with a packing fraction of 82% and an allowable bending radius of 1 in. (25 mm).

The numerical aperture of the fiber bundle is 0.35, requiring lens positioning shown in the assembly figures 12 and 15.

Three fiber assemblies were procured:

a) Input cable (from the light source to the sensor)
b) Signal cable (from the directly transmitted beam, crossed-polarizer, to readout)
c) Reference cable (from the reference beam, parallel polarizers, to the readout (detector #3)

Both output cables were bifurcated to allow for investigation and measuring separately of AC and DC components and connection to sensors responding to different wavelengths.

The READOUT SYSTEM (See Ch. 4 below) explains more in detail the function of the 4 outputs.

3. TESTING PROGRAM AND TEST DATA

In the research program detailed above, a significant portion of time and effort was dedicated to the experimental verification, included:

1. Designing of suitable experiments and test set-up required to perform the evaluation.

2. Running the test

3. Tabulation and evaluation of test results

The testing was designed to:

a. Evaluate the stress field in the projected design, using a photo-elastic model, for geometry optimation.

b. Evaluate the material performance and measure Brewster constant at elevated temperature.

c. Evaluate efficiency of polarizers

d. Evaluate the performance of the readout system at various stages of its completion.

e. Evaluate the overall sensor and housing performance, at various completion stages.

Test results of (a), (b), and (c) were reported within paragraphs related to these topics. (See 2 above)

The test of the overall system performance was carried out in two stages:

3.1. Testing of the Fused Silica Sensor

Upon completion of the design work, a fused-silica sensor (see figure 13) was assembled in its housing and tested at room temperature at internal pressure of 0 to 500 psi using the set-up shown in figure 28.

The stress birefringence vs. applied pressure was measured first using a transmission-polarimeter, using the SENARMONT method. The table below summarizes the results of this test.

BIREFRINGENCE AND STRESS IN THE TRANSDUCER VS. PRESSURE

Pressure psi	Birefringence in the sensor N (fringe order)	Stress at the measured point in the transducer $\sigma = \frac{NC}{t}$ psi
0	-.02	-50
50 100	.01 .035	100
150 200	.07 .10	290
250 300	.13 .16	460
350 400	.19 .23	670
450 500	.25 .29	850

σ	stress at the point of measurements (psi)
t	thickness crossed .368 inches.
C	Brewster constant of fused silica.
N	measured fringe order ($N = \delta/\lambda$).

The maximum measured fringe order N = 0.29 is in EXCELLENT agreement with our target (.30) and demonstrate the validity of the model results. This result also illustrates the merits of the model approach and the ability to develop directly an accurate design.

The measured stress at the Top-of-the-Rib location was 850 psi. This stress level is acceptable in fused silica. The nominal stress in the cylinder at 500 psi internal pressure was:

$$\sigma = \frac{pd}{2t} = 1580 \text{ psi}$$

and the nominal difference of principal stresses.

$$\sigma_1 - \sigma_2 = \frac{pd}{4t} = 790 \text{ psi}$$

The measured output at the Top-of-the-Rib was, therefore, higher than the cylinder output, confirming again the RIB optimation procedure.

Anticipating a stress concentration factor of 3 to 4 in the flange fillet, the maximum stress in the body of the sensor would become $3 \times \sigma_3 = 2370$ to $4\sigma_3 = 3160$ psi

In order to eliminate the cracking problems at the flange fillet, the sensor was tested using the pressure port p_1, subjecting the body of the sensor and the gasket to compression.

3.2 Readout System Calibration and Testing

Upon completion of the evaluation of the sensor, a calibration test was performed to evaluate the response of the readout system using a calibrated birefringence. To perform this test, the sensor was removed from the housing and a tensile specimen was placed between the input and output polarizers.

The readout system received from Aurora was set-up, collecting the ouput from the transmitted beam (TB) (crossed polarizer) and reference beam (RB). The results of this evaluation are shown on the figure 29.

These test results show a good performance of the amplifier, of the light source, and also demonstrates that the form of the output of $\sin^2 \frac{\pi \delta_i}{\lambda}$ and $\cos^2 \frac{\pi \delta_i}{\lambda}$ properly represents the output.

It also shows that polarizer inefficiency and the zero-offset must be accounted for in the final algorithm translating the measured photodiode outputs into pressure.

As a result of this calibration test, the readout system was modified, to eliminate some of the light leaks producing a cross talk between the channels. Some gain-resistors were changed to eliminate the possibility of saturation, and also to match the input-resistance requirements of the logic IC used.

3.3. Testing at Elevated Temperature - 600° C Test

In the first phase of the testing program, the complete transducer body was immersed in high-temperature environment, simulating the engine-compartment temperature.

The output was measured as a function of pressure and temperature at pressures of up to 500 psi and temperatures up to 600° C.

Also, temperature-measuring channel output (PD4) was used to indicate the temperature. The figure (30) below shows the output of the transmitted beam TB (detector PD1) and reference beam RB (detector PD3) vs. pressure at maximum temperature of testing, 600° C.

The output of PD1 and PD3 vs. temperature was negligible. The output of PD4 vs. temperature is shown on the figure (31). This photodiode was incorporated in the system to provide temperature indication. The expected use of the temperature indication was to implement a corrective term in the algorithm for extraction of pressure from PD1 and PD3 measured voltages.

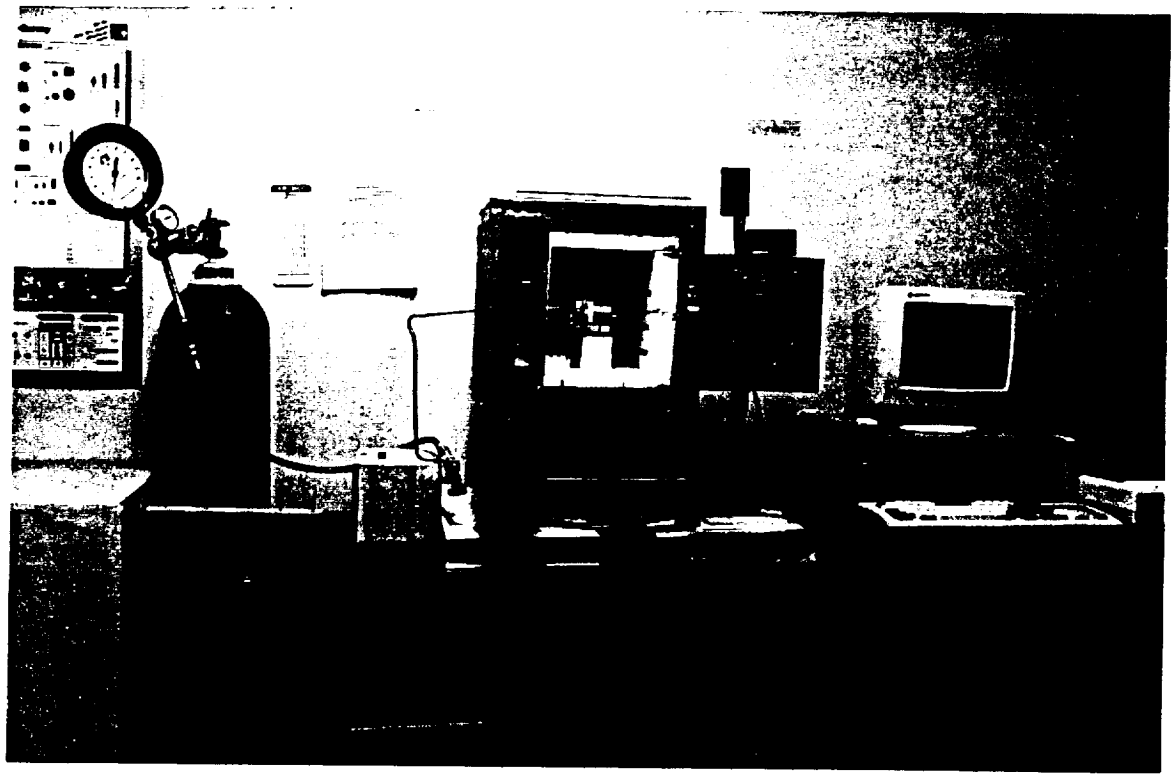

Fig. 28. Testing of the Fused Silica Sensor

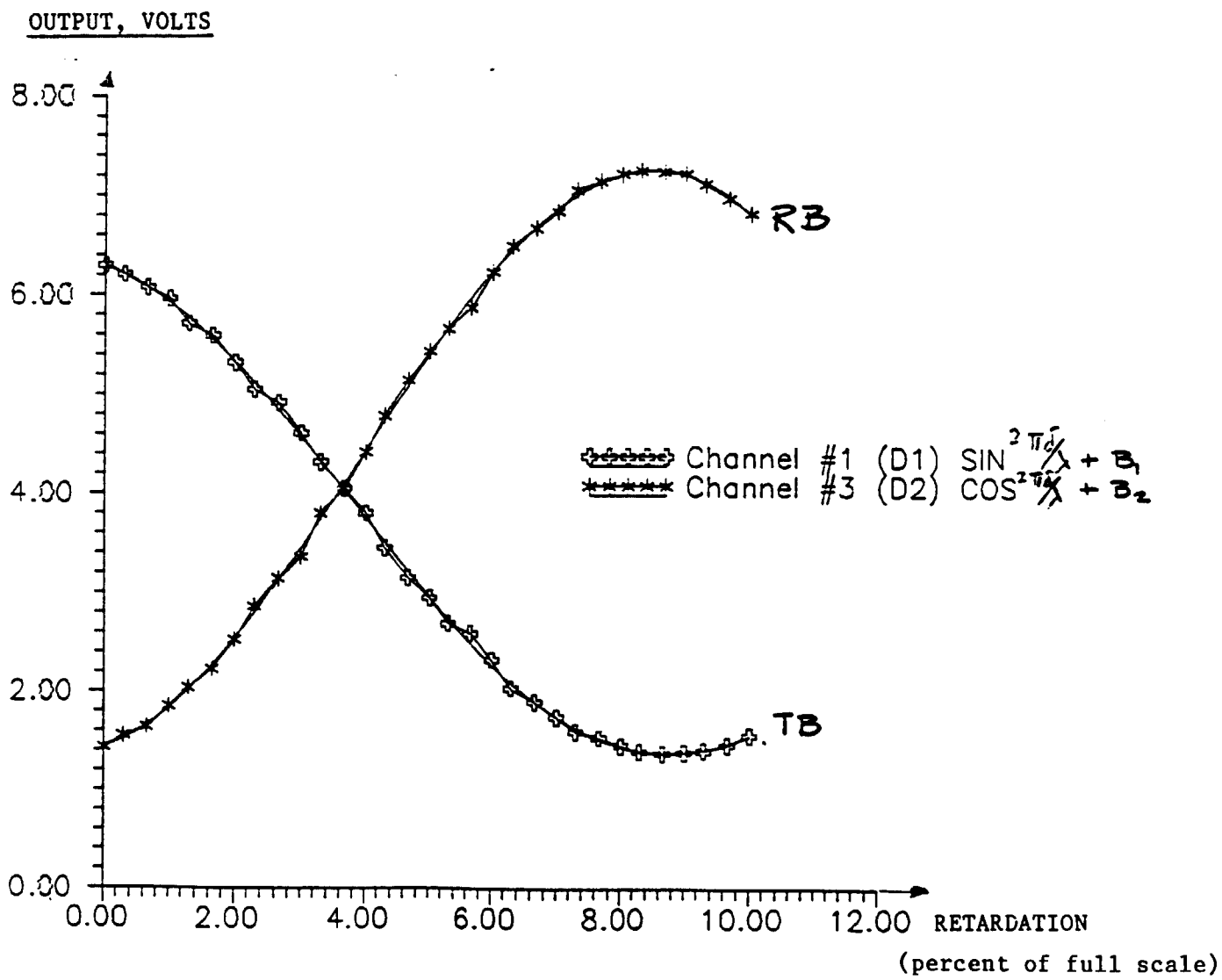

Fig. 29. TB and RB Output vs. Retardation

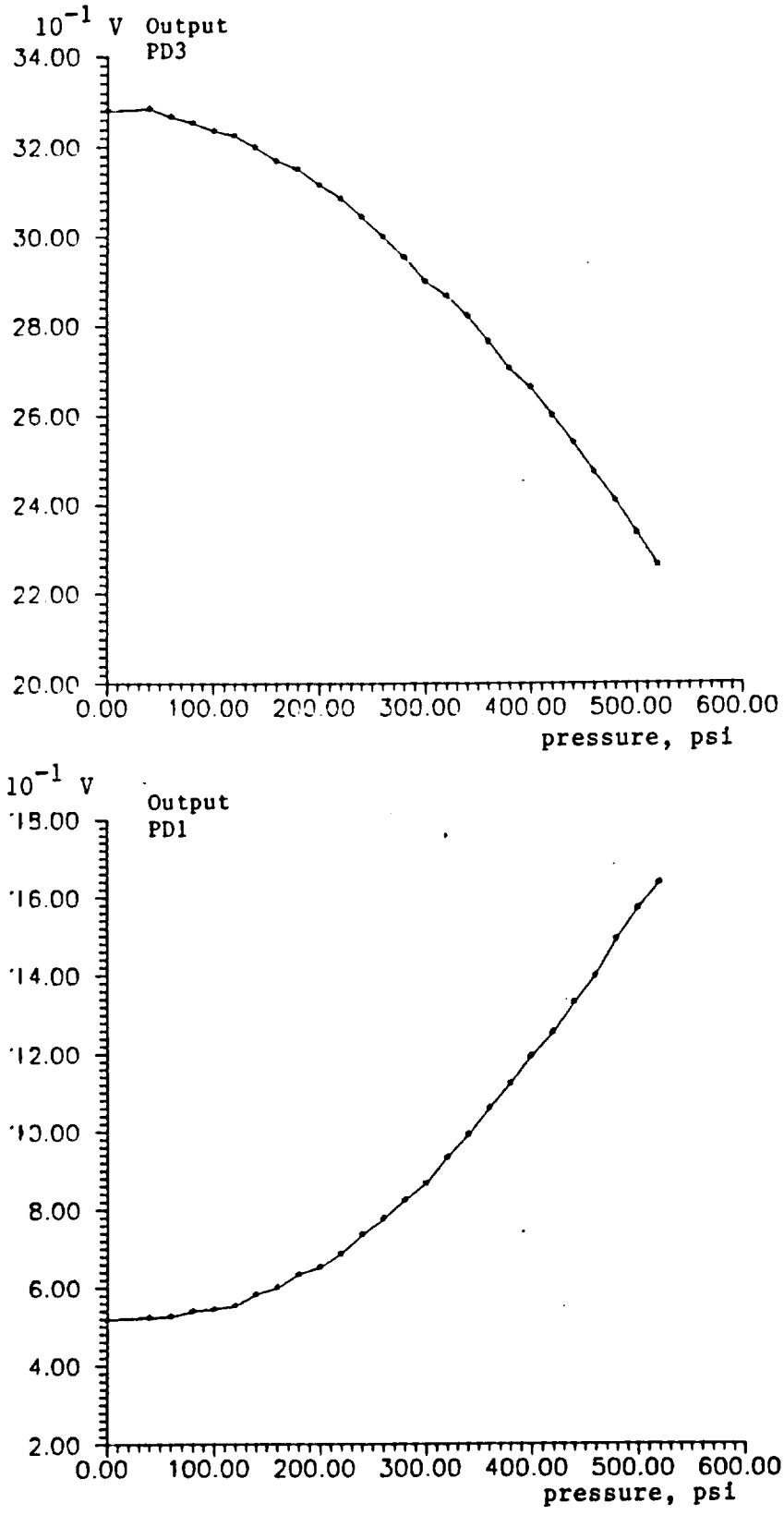

Fig. 30. Output (Volts) of Photodetector PDI & PD3 vs. Pressure.

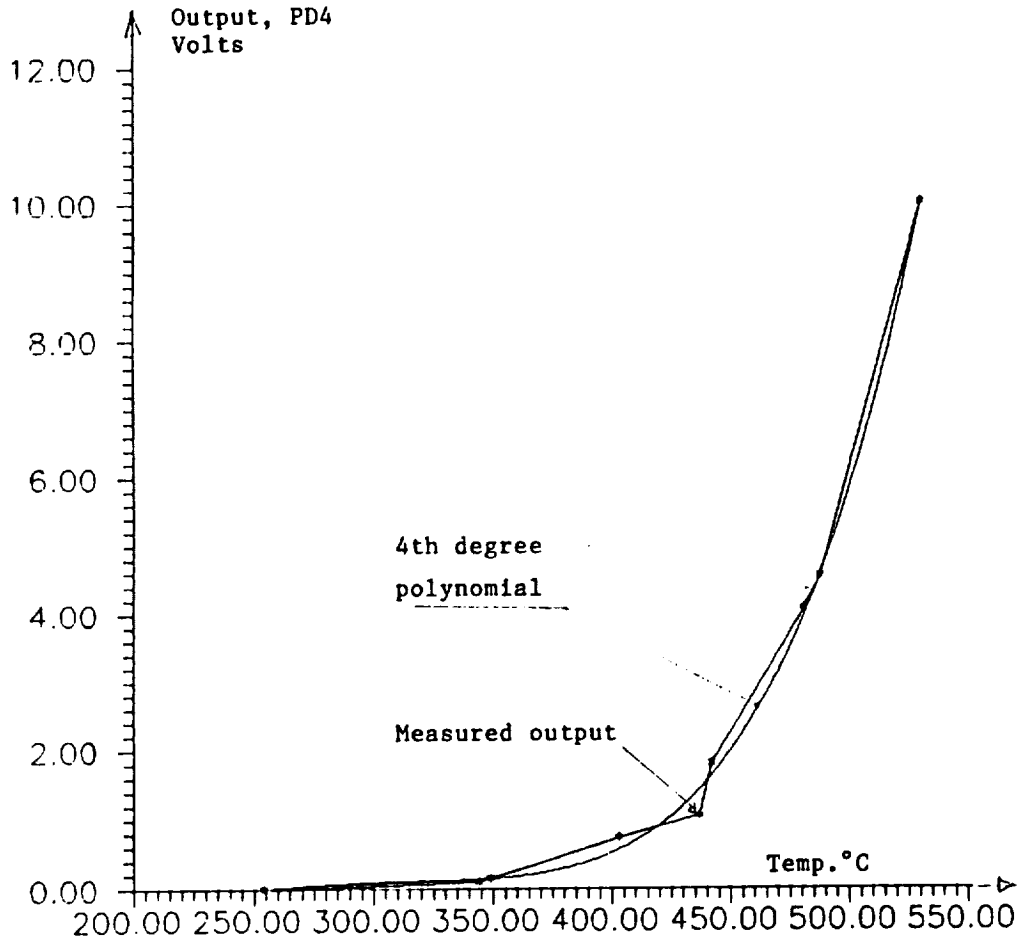

Fig. 31. Ouput of PD1 Photodetector vs. Sensor Temperature

3.4. Final Test - 1500° C Gas-Pressure Measurement

For the final test, measuring the gas pressure with the gas temperature at 1500° C, it was first necessary to design a set-up producing 1500° C temperature, at pressure ranging up to 500 psi, while the body of the transducer remained at the engine compartment temperature generating, therefore, a substantial temperature gradient within the transducer itself, and producing the most adverse functioning condition.

3.4.1. High-Temperature Gas Generating Set-Up

The concept of the high-pressure 1500° C-temperature gas supply was solved using a high-pressure nitrogen container with a precision regulator as a source of pressure, and a specially developed oxy-acetylene furnace pre-heater, to supply the 1500° C gas to the test chamber (figure 32).

The system shown in a cross-section in Figure (32) and in actual set-up, figure (33), includes:

-High pressure nitrogen, supplied with a pressure regulator

-An oxy-acetylene burner, heating the combustion chamber to the required temperature and the heat-exchange coil for pre-heating the pressurized nitrogen to 1500° C.

-A precision gage for measuring the pressure at the transducer port.

-A thermo-couple measuring the nitrogen temperature at the transducer input.

The molybodenum heat exchanger pipe carrying the high-temperature gas to the transducer was ¼" O.D. Although the molybodenum oxidizes rapidly at 1500° C, we maintained a reducing environment, feeding a small flow of pressurized nitrogen inside, and maintaining an acetylene-rich flame in the combustion chamber.

The pre-heater and heat exchanger were mounted immediately adjacent to the 600° C furnace, maintaining the transducer housing at constant temperature, simulating the engine compartment temperature.

The entire set-up was performing extremely well and permitted measurement of the output of the completed sensor assembly. The results of multiple tests run at gas temperatures ranging from room temperature to a maximum of approximately 1520° C, is shown in figure 34. This figure clearly demonstrates that:

a. The birefringent sensor performed repeatably

b. The output is independent of temperature

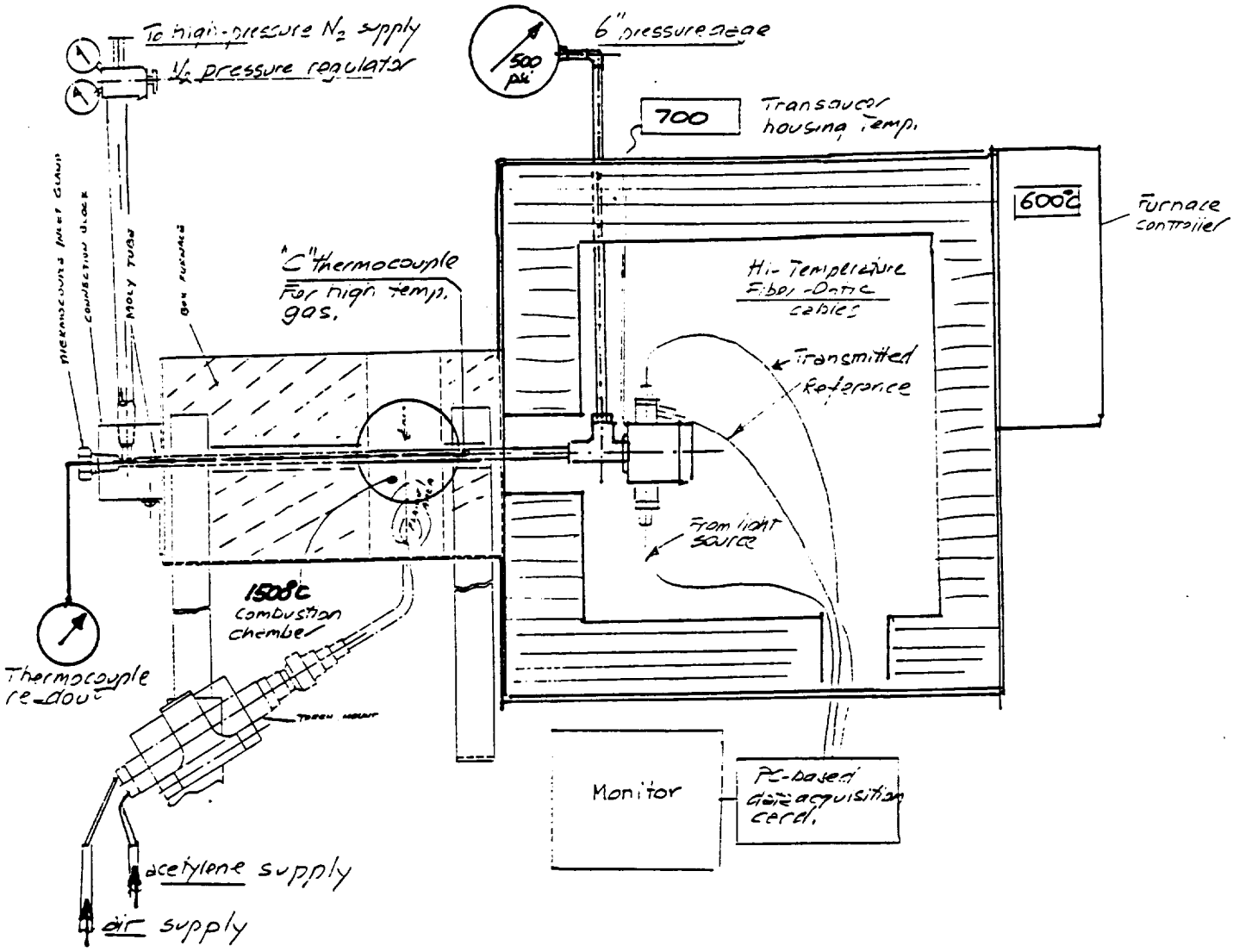

Fig. 32. High-Temperature Pressured Gas Generator and Instrumentation Schematic for Final Test of the Pressure Sensor

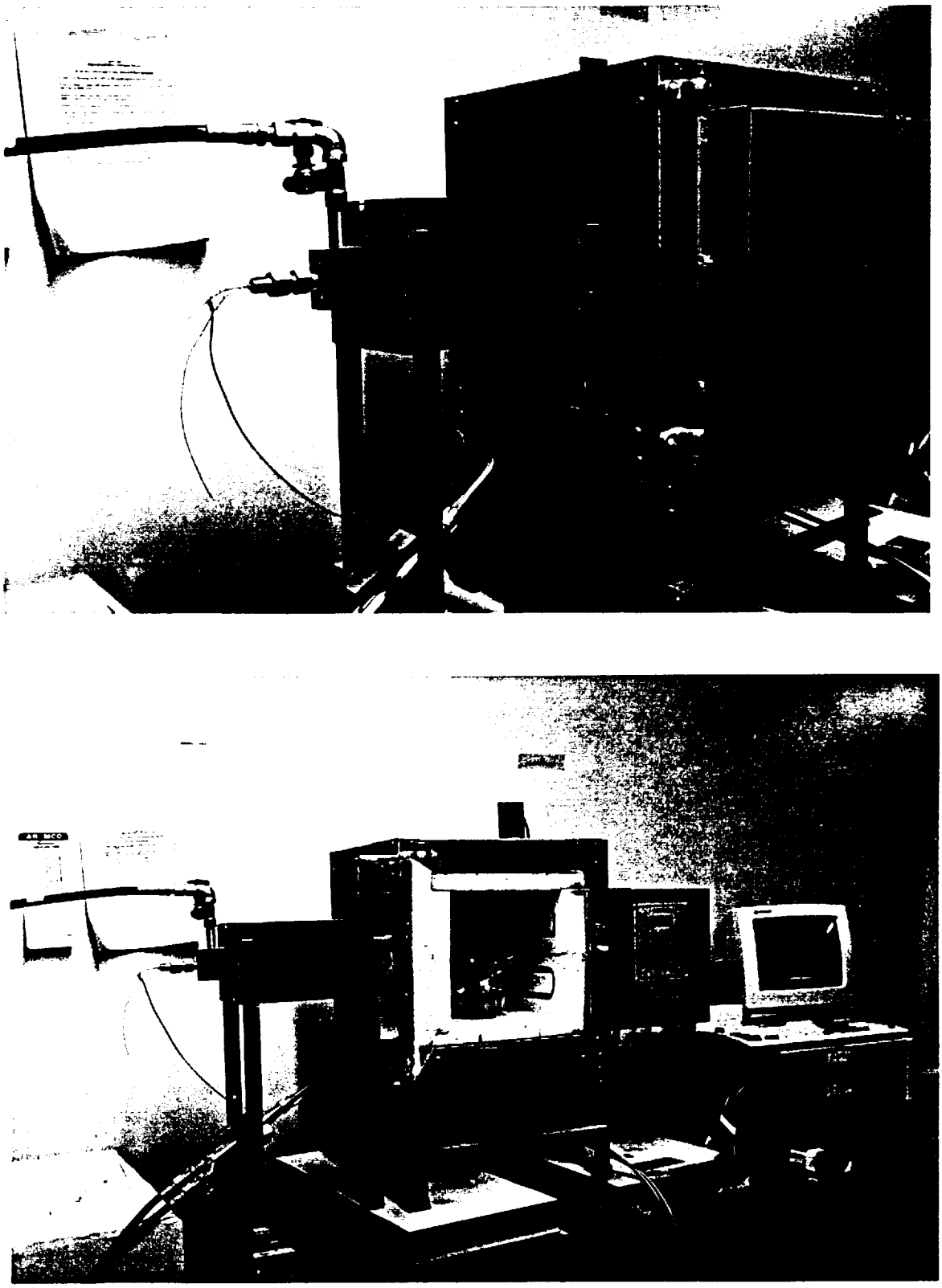

Fig. 33. Final Testing Set-Up

c. The test set-up performed in accordance with its design objectives and permitted testing of the sensor output within the specified range.

The sensor outputs (figure 34) were used for programming of the software of the readout system, for direct readout.

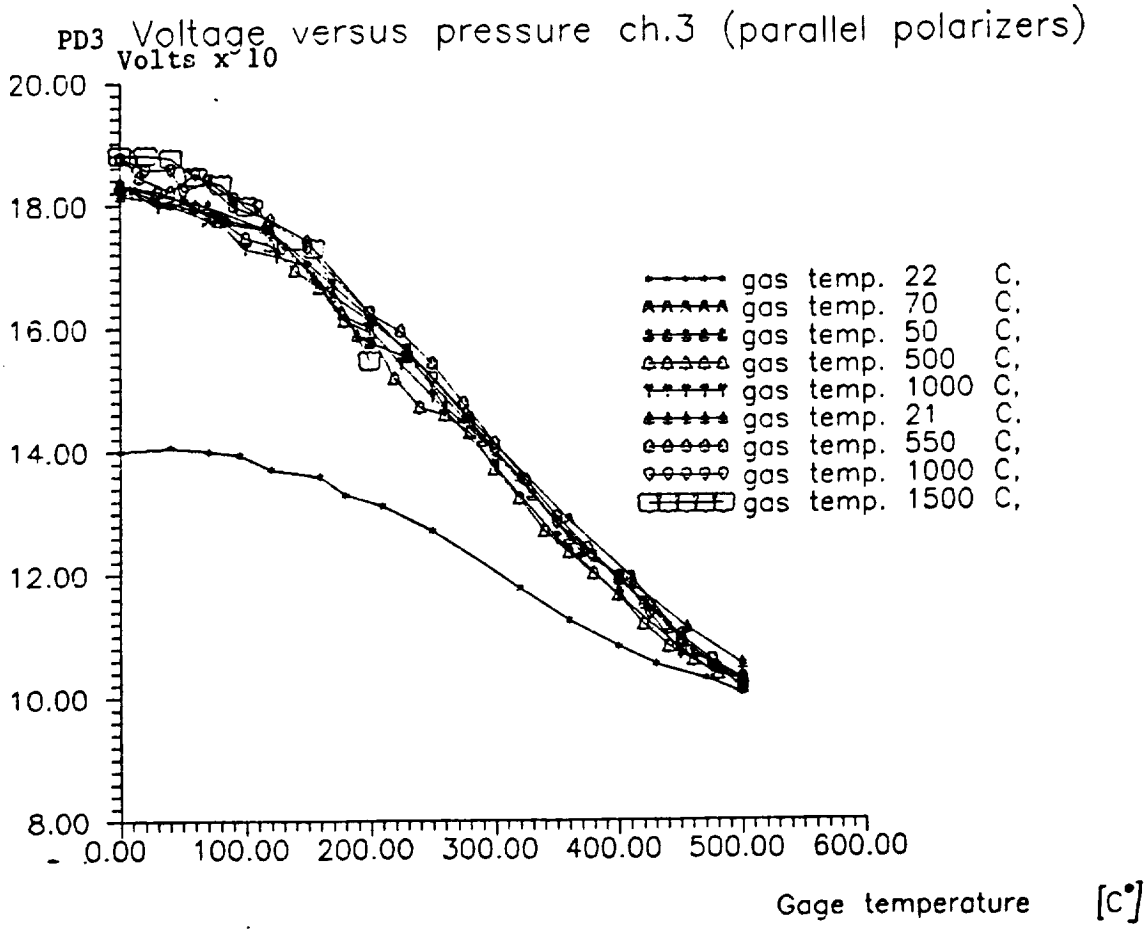

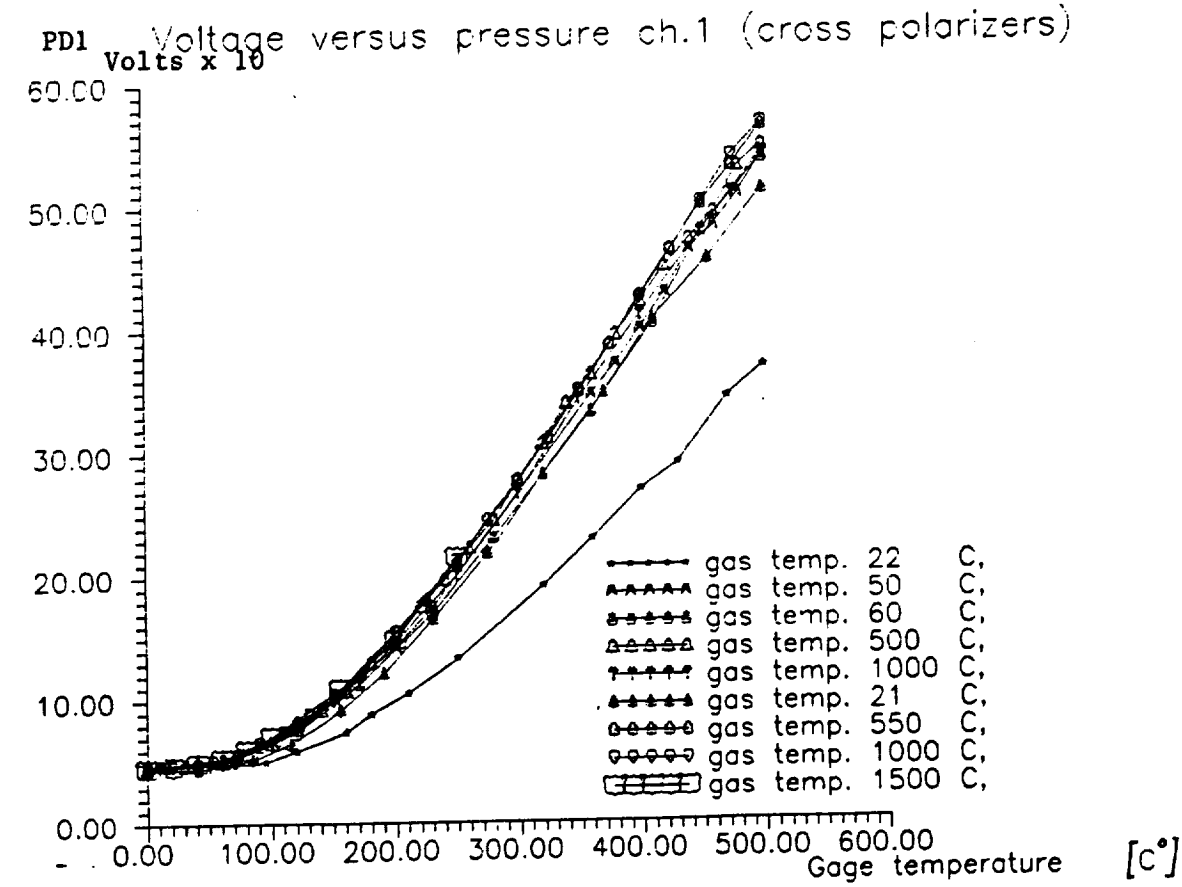

Fig. 34. Readout-Output (Volts) vs. Pressure, psi

4. ELECTRONIC READOUT SYSTEM

The electronic readout system was a PC-based opto-electronic interface designed using the parallel reference beam method for control of power variations in analog sensors. As described more fully in Appendix II, the system provided all opto-electronic functions on a plug-in board within 286 processor. All logic functions were performed by the PC. Menu-driven operation of the system was viewed on the monitor display.

As suggested by the schematic diagram in figure 35, the electro-optic interface card included the following functions:

a. Single Light Source
b. Three Parallel Detectors
c. AC and DC-Coupled Amplifier Stages
d. A/D Converter and analog multiplexer

4.1. Light Source

For this function a high-brightness infrared LED, emitting at 840 nm, was used. The choice of wavelength was made to optimize launched power and reliability. In addition, it provided a reasonable compromise between the long wave region, where substantial thermal radiation might be expected to interfere with analog power measurement, and the visible region, in which solid state sources with high power were not available. In addition, the 820 to 850 nm range is one of minimum fiber attenuation. The cost, finally, of near-infrared sources was modest.

The source emission was modulated at 10 kHz, 50% duty cycle. This allowed the receiver to filter out dc background power variation independent of the sensor signal. In addtion, pulsed mode operation allowed the source to oerate at a higher power level.

4.2. Detectors

Three solid state detectors were installed in the electro-optic interface for the parallel detection of transmitted, reference, and thermal background signals:

-PD1. Si PIN diode for reception of the transmitted signal at 840 nm.
-PD3. Si PIN diode for reception of the reference signal at 840 nm.
-PD4. InGaAs PIN diode provided for the measurement of the thermal DC background in either the transmitted or the reference beam cable, at the user's option.

4.3. Amplifier Stages

The signals from each of the three photodiodes were amplified by JFET op-amps with gain, shielding, and filtering designed to optimized the desired signal from each. The output from the first silicon photodiode, PD1, after preamplification, was filtered both AC (high pass) and DC. These two signals then passed through further stages and were input to the analog multiplexer. The AC signal was designated "channel 1" and represented the principal transmitted sensor-modulated beam, which in the sensor had passed through the crossed polarizer path. The second,

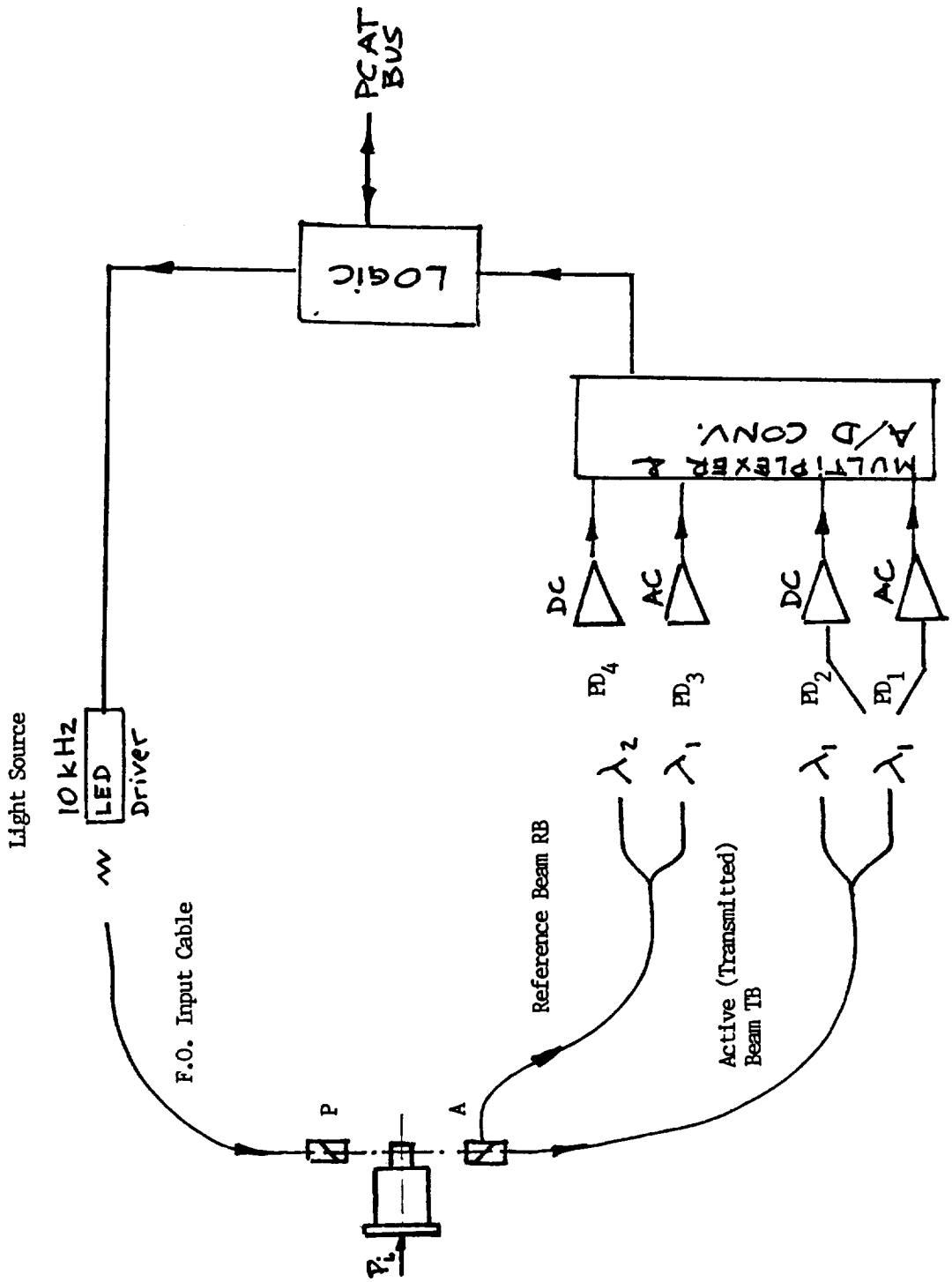

Fig. 35. Circuit and System Layout

DC signal was input as "channel 2". This signal was available for the measurement and calculation of sensor temperature from the short wave (SW) thermal radiation region (below 1100 nm, as detectable by silicon). It would be interrogated only during times when the source LED was turned off.

The output from PD3 was AC-coupled only. After amplification it was input to the multiplexer as "channel 3". This signal represented the sensor-modulated reference beam, which in the sensor had passed through the parallel polarizer path.

The output from PD4, after amplification, was low-pass filtered. Thus only the DC component of optical power from this broad-band detector was utilized, for the measurement of temperature. This signal was identified as "channel 4" at the multiplexer. Channel 4 was interrogated only during periods when the light source was turned off by the computer.

4.4. Analog Multiplexer

This four channel multiplexer directed the signals from channels 1 through 4, in sequence, to the A/D converter. Timing and sequencing were governed by the host computer through a tri-state buffer/driver and a flip flop.

4.5. A/D Converter

This 12-bit device digitized the outputs from the four channels, in sequence, for further processing by the computer.

4.6. Readout Operation

The host computer actively controlled the sequencing and data acquisition from the electro-optic interface board. In operation this process included the following elements.

The source LED was turned on for certain periods, in 10 kHz pulsed mode. During these periods data was acquired from channels 1 and 3. While the LED was turned off, data could be acquired from channels 2 and 4. The correspondence of passive optical sensor, signal, diode, and channel was as follows:

Cable Designation	Optical Signal	Diode	MUX Channel
TB1	TB1-AC-1	PD1	1
	TB1-DC-1	PD1	2
RB1	RB1-AC-1	PD3	3
TB2 or RB2	TB2-DC-2 or RB2-DC-2	PD4	4

The three high-temperature fiber-optic bundle cables were connected as follows:

simplex cable from source LED to sensor input

TB was a bifurcated cable for the transmitted principal data beam. Simplex end attached to sensor output. One branch (TB1) attached to PD1; second branch optionally attached to PD4.

RB was a bifurcated cable for the reference beam. Simplex end attached to sensor reference fitting. One branch (RB1) attached to PD3; second brach optionally attached to PD4.

The host computer initiated data logging by latching on and off instructions for the LED Into the flip-flop. The instruction designated each of the four data channels to be read, in sequence. When the instruction set required LED power, a 14-stage counter provided a timed signal, which, amplified, excited the LED.

At the same time, and depending on sequence, the host computer interrogated the A/D converter. The status byte from the A/D was stored in the tri-state buffer/driver. If the status was "ready", the computer read the 12 bit data for the designated data channel.

The reading of data bytes from the A/D converter automatically initiated conversion of another sample. The computer logged data from all four channels and processed the data using the program listed in Appendix III. The output displayed on the monitor was pressure, as calculated from the values of channels 1 and 3. The data from channels 2 and/or 4 could be utilized, if desired, for the calculation of sensor temperature.

4.7. Algorithms Used in Programming

It was demonstrated throughout the test program, that:

a. The output of the birefringent sensor is best represented by its theoretical output.

$$I_1 = Io_1 \cdot \sin^2 \frac{\pi\delta}{\lambda} \qquad \text{(transmitted beam)}$$

$$I_3 = Io_3 \cos^2 \frac{\pi\delta}{\lambda} \qquad \text{(reference beam)}$$

Where I_{o1} and I_{o3} are amplitude related to the same source Io and fluctuating proportionally to the changes of the source intensity.

In addition to I_{o1} and I_{o2}, there is an offset due to the polarizer inefficiency, in the form of a constant B_i.

$$I_1 = I_{o1} \left(\sin^2 \frac{\pi\delta}{\lambda} + B_1\right)$$

$$I_3 = I_{o3} \left(\cos^2 \frac{\pi\delta}{\lambda} + B_3\right)$$

The final constant represents the birefringence offset δ_o introduced intentionally, to eliminate the dead-band near the $\delta = 0$ region, yielding the final expression to become:

$$I_1 = I_{o1} \left[\sin^2 \frac{\pi(\delta + \delta_o)}{\lambda} + B_1\right]$$

$$I_3 = I_{o3} \left[\cos^2 \frac{\pi}{\lambda}(\delta + \delta_o) + B_3\right]$$

or expressed in terms of pressure :

$$I_1 = I_{o1} \left[\sin^2 \frac{\pi}{\lambda}(\delta_o + K_p P_i) + B_1\right]$$

$$I_3 = I_{o3} \left[\cos^2 \frac{\pi}{\lambda}(\delta_o + K_p P_i) + B_3\right]$$

The calibration constants I_i , B_i and Kp must be derived from the experimental results. These constants must fit all points of the calibration curve and can be derived analytically from discrete points or using multitude of points and least-square fitting algorithm.

In the electrical regime I_1 and I_3 were represented by the outputs of channels 1 and 3, respectively. In processing the data, the functions derived above were converted to the form:

$$\text{Ch. 1} = K_{11} * \sin^2 [K_{12} * P + \delta_1] + K_{13} \quad \text{(channel 1, volts)}$$

$$\text{Ch. 3} = K_{31} * \sin^2 [K_{32} * P + \delta_3] + K_{33} \quad \text{(channel 3, volts)}$$

In the above equation, the measuring of the co-efficients K_{ij} is the following:

K_{11} and K_{31} are full scale amplitudes in volts

K_{12} and K_{32} are the K factor of the sensor at the measurement location, in psi^{-1}. Ideally, when the curve fitting is performed these two parameters should be identical.

δ_1 and δ_3 are the residual phase shift in the sensor, due to non-zero residual stress at the measurement location, in units of wavelength. Ideally δ_3 should be larger than δ_1 by exactly $\pi/2$.

K_{13} and K_{33} are the vertical offset, or voltage baseline, of each curve, in volts. This offset is due to circuit noise, polarizer inefficiency, and other factors.

It will be noticed in the above electrical functions that the sine squared function has been utilized for both outputs. This has been arranged by adding $\pi/2$ to the value of δ_3, which by trigonometric identity allows the substitution of $\sin^2$ for $\cos^2$.

In the development of the readout system a computer-based least-squares curve fitting program was used to find the best fit of these analytical functions to the experimental data. The data shown in figure 34 were first averaged, to identify the best fit which would be independent of temperature. This average omitted the first run, at 22° C, which clearly preceded a "burn-in" of the system. Manual estimation of the function parameters was performed for a first-shot curve fit. Then the regression software was used to arrive at the following values:

K_{11} = 6.587758 volts
K_{12} = 0.5837 psi^{-1}
δ_1 = -9.5987 nm
K_{13} = 0.462104 volts
K_{31} = 0.881239 volts
K_{32} = 0.6666 psi^{-1}
δ_3 = 16.8251 nm + $\pi/2$
K_{33} = 0.970706 volts

Ch. 1 = 6.587758 * $\sin^2$ [0.002183 * P + (-0.035899)] + 0.462104

Ch. 3 = 0.881239 * $\sin^2$ [0.002493 * P + 1.633722] + 0.970706

Using these values, the pressure was calculated from the function:

$$P_i = (1/K_{i2}) * [\sin^{-1} \frac{(\text{Ch. } i - K_{i3})}{K_{i1}} - \delta_i]$$

It will be noticed that $K_{12} \neq K_{32}$, and $\delta_1 = \delta_3 \pm \pi/2$. This is of less concern than might be expected, however. For instance, the residual phase shifts are both so close to zero, compared with the wavelength of 840 nm, that neither is significant in the overall curve fit. Both are less than 0.02 wavelength in magnitude. The difference between the two K-factors is more signficant, but with both curves fit to an extremely high degree of accuracy the difference is immaterials to the function of the readout system for the measurement of pressure.

5. DISCUSSION OF RESULTS AND CONCLUSIONS

In the course of the research work performed, the following results were accomplished:

-A new design of photoelastic pressure-transducer, capable of performing measurements of gas-pressure at temperatures of up to 1500° C was developed.

-A new design of a general-purpose, integrated, readout interface for fiber-optic sensors was developed. This electronic readout was formatted into a self-contained PLUG-IN, fitting a standard PC-AT bus format, including ON-BOARD light source, reference and active beams amplifiers, multiplexing readout and logic required to operate the system.

-A voluminous research work was performed, resulting in characterization of several photoelastic materials suitable for use in high-temperature sensor technology. The Brewster constant of these materials is now available, both at room and elevated temperatures.

-Design of high-temperature seals was improved, insuring constant bolt forces, to avoid cracks in brittle materials subjected to gasket forces.

These fundamental advances permitted the final design of the sensor, that performed its specified functions.

In order to evaluate the photoelastic material properties at elevated temperature, a fixture was designed, that permitted subjecting the calibration specimen to dead weight at elevated temperature.

Also a heat exchanger for heating the pressurized gas was designed.

While most of the research objectives were accomplished, some of the problems remained unsolved, in particular:

-Fiber-optic links used did not satisfy the manufacturer's specifications and exhibited a significant deterioration when operating BELOW their specified maximum operating temperature.

-Crystal-polarizer efficiency did not perform in accordance with the manufacturing specifications, making their use difficult and perhaps leading to practical problems in their implementation.

Undoubtedly, once sufficient advances in high-temperature fiber-optic technology and polarization-preserving fibers are accomplished, the results obtained and the transducer design developed will become not only more accurate, but also more economical.

REFERENCES

1. Wesson, L.N. "High-Sensitivity Photoelastic Pressure Sensor", Proceedings of FIBER/LASER '86 SPIE, Boston, MA, 1986.

2. Redner, A.S. and Wesson, L.N. "Fiber-Optic Photoelastic Pressure Sensor for High Temperature Gases".

3. Jessep, H.T. "On the Tardy and Senarmont Methods of Measuring Fractional Relative Retardation", British Journal of Applied Physics, 4(5), pp. 138-141, 1953.

4. Redner, A.S. "Model Approach in Structural Design", Proceedings, ASCE National St. Conference, 2205, Cincinnati, OH, 1974.

5. "Fiber-Optic Components", Dolan-Jenner, Woburn, MA, 1987.

APPENDIX I. SUMMARY OF PHASE I RESULTS

In Phase I theoretical and experimental development and analysis was performed to demonstrate the potential for photoelastic measurement of pressure at high temperatures. The basic mechanical configuration of the baseline sensor was that of the bending plate.

The theoretical research effort included several tasks:

-Evaluation of alternative sensor materials. Among the twelve candidates considered, most presented difficulties of optical orientation, availability, or fabrication. The strongest candidates were sapphire and fused silica. Of these, fused silica was chosen for the feasibility model.

-Evaluation of various means of polarizing light within the high-temperature environment of the sensor. The means considered included the pile-of-plates, dielectric film, and first-surface Brewster reflection. In the model the first-surface approach was demonstrated, using a prism fabricated of fused silica and reflection at Brewster's angle.

-Evaluation of alternate forms of fiber-optic cable. Alternatives included multimode fiber with special coatings, polarization-maintaining fiber, sapphire fiber, and a road light guide. Of these, the second and third were felt to introduce undue risk into the Phase I project. Therefore the model was tested using mutlimode fibers for most of the optical path and a silica rod light guide for transmission within the extreme temperature environment.

-Evaluation of alternate approaches to the electro-optic interface and signal processing. Problems to be addressed included variable attenuation effects in the cables and background power variations due to thermal radiation. Methods of addressing these effects included the use of short wave emitter and detector, narrow-band filtered optics, pulsed source modulation, parallel output fibers, and the use of two wavelengths. For the feasibility model existing equipment directed the use of ordinary DC-mode single wavelength operation. In a subsequent test, however, the efficacy of pulse-mode operation and two-wavelength calibration was demonstrated.

At the conclusion of the theoretical research tasks, a feasibility model pressure sensor was designed, built, and tested. The approach used in the model was the bending plate method.

Temperature exposure testing of the various sensor components confirmed that all were capable of operation both at, and after, exposure to temperatures up to 650° C. The active element, polarizer, and light guide were all fabricated of fused silica. Most of the housing parts were fabricated from stainless steel, and the pressure seal was based on graphite. Reflection and polarization of light from the fused silica components was virtually unaffected by the exposure.

The complete sensor was tested for optical response to various pressures up to 400 psi, while uniformly heated to temperatures from 25 to 650° C. It was found that the optical intensity was successfully modulated according to a sine squared function over a dynamic range of roughly 10 to 1. The pressure at which peak optical power was transmitted was 180 psi. The dynamic range changed by only 10 percent as the sensor temperature was increased from 25 to 620° C, and the point of peak pressure did not change at all, within the limits of experimental error. These results suggested that the sensor concept was materials-limited only in its range of application.

Based on these results it was concluded that a Phase II development effort would have a strong probability of resulting in a successful engine-mountable passive optical sensor.

AURORA MODIFIED EIU

The AURORA modified electronic interface unit (EIU) consists of four sections: light source, detector, data acquision, pc-bus interface. The EIU has been built in a pc pluggable board.

1. Light Source

In this transmitter configuration, a buffer gate (U8) drives a transistor (Q1) which turns ON and OFF the LED (D8). When the input to the gate is low, the transistor is turned off and a load resistor at collector supplies the desired current. In this modified EIU, only one 850 nm LED is used for light source. This LED drives both the sensor and the reference filter.

The signal is transmitted at 10 KHz rate, with 50 % duty cycle. The pulsing insures that the LED signal may be distinguished from black body radiation generated in the sensors. Black body radiation changes relatively slowly with time and thus may be considered as DC in nature. Therefore by turning ON and OFF periodically, the separation of the AC transmitted signal component from the DC temperature component is possible. Turning ON and OFF 10 KHz pulses is controlled by a command issued from the host PC.

In order to compensate for LED temperature coefficient differences, a reference fiber line is also provided for the sensor which is fed back to a silicon diode detector and transimpedence amplifier stage.

2. Detector

The returing light is detected by a set of PIN photodiode and transimpedance amplifier modules. The basic principle of operation is that, an incident photon creates a hole-electron pair near or within the depletion region of the semiconductor. The electrical field then separates the hole-electron pair and causes current to flow in an external circuit. Therefore, The pin diode is operated in its photoamperic mode where it is highly linear (i.e., zero bias voltage). The PIN diode behaves as a light controlled current source in this mode. The detector circuitry consists of three PIN diodes; one for 850 nm AC/DC signal (D1), one for 1300 nm long wave signal (D3), and one for the reference signal (D2). The AC/DC signal is separated into AC signal and DC signal after a transimpedance amplifier (U1). The transimpedance amplifier (U1, U3, and U5), using a differential input mode, converts the PIN current to a corresponding voltage.

The signals are then amplified and/or rectified by the circuit surounding U2 and U4.

3. Data Acquisition

The signals are sorted into the following four channels:

Channel 3 = long wave dc
Channel 2 = reference ac
Channel 1 = 850 nm dc
Channel 0 = 850 nm ac

The amplified input signals are then multiplexed by a 4-channel differential analog multiplexer (U6). Analog-to-digital conversion takes place with a 12-bit A/D converter (U7).

4. Bus Interface

PC/AT can start or stop transmitting light to the sensor by executing an instruction of "OUT 720 (Hex Port #), command byte". Command byte is defined as follow and latched into U12:

Bit Position	Description
(MSB) 7 to 4	not used
3	Start(1) / Stop(0) the Board
2	Transmit On(1) / Off(0)
1	Channel bit 1
0	Channel bit 0

Channel bit 1 and bit 0	Channel number
00	Ch 0
01	Ch 1
10	Ch 2
11	Ch 3

The host PC/AT can poll the status of the A/D converter by executing an instruction of "IN AL, 730 (Hex Port #)". The status byte is stored in U11. The bit designation is as follow:

Bit	Description
3	Transmit On(1) / Off(0)
2	Data Ready(0) / Not Ready(1)
1	Channel bit 1
0	Channel bit 0

If 'Data Ready' bit is "0", the analog-to-digital converter has finished the conversion and data is ready to be read for the channel number indicated by ch1 and ch0 bits.

Data can be read by executing an instruction of "IN AX, 720 (Hex Port #)". Register AL will have 8 most significant bits and register AH will have 4 least significant bits trailed by 4 zero bits.

Reading data bytes from the A/D converter automatically initiates a conversion for another sample. Therefore, a care should be taken. If the next channel should be sampled after current channel, that next channel should've been specifed before reading data bytes for the cuurent channel by executing an "OUT 720 (Hex), AL', AI with the command byte.

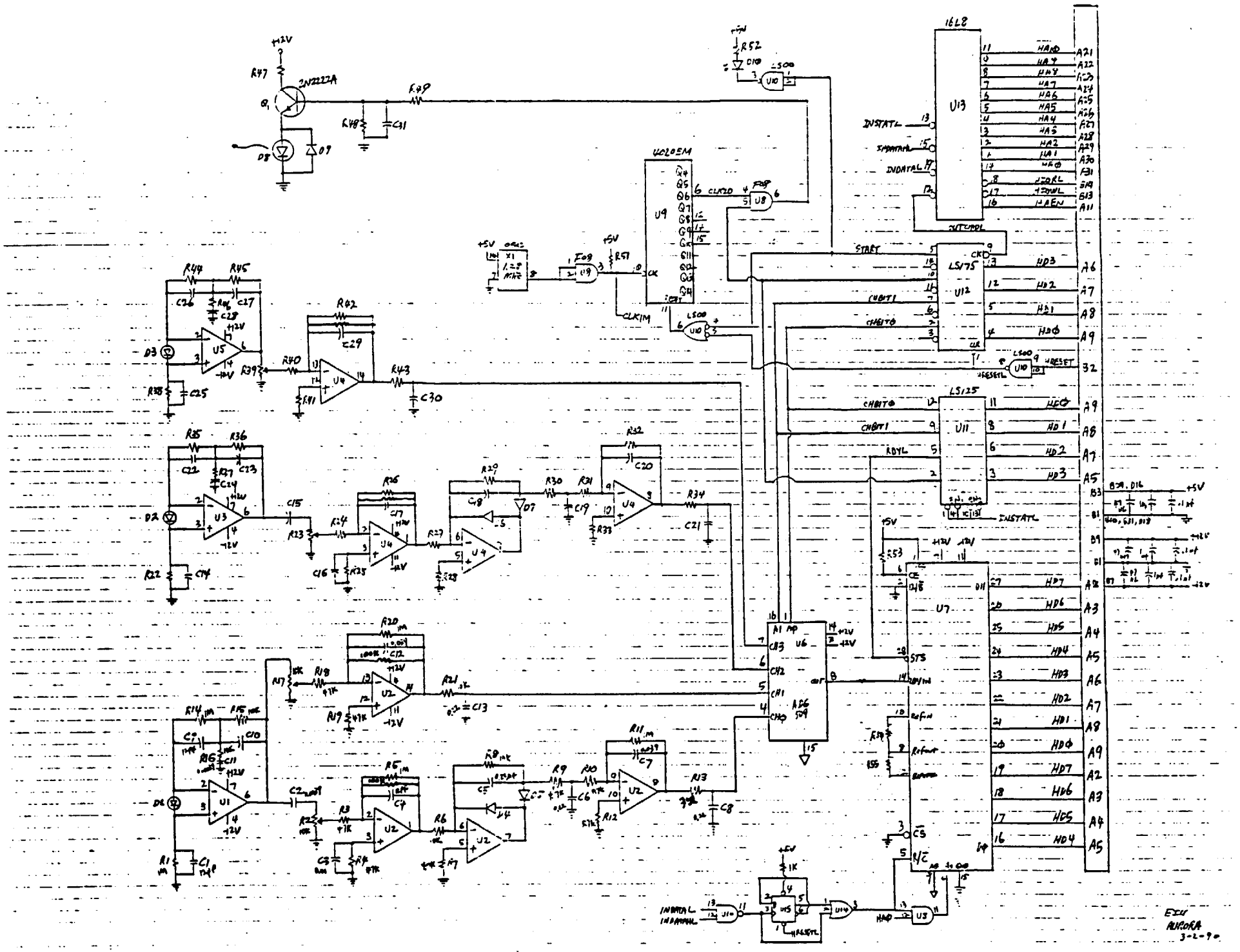
2N2222A
LS00
LS74
LS75
LS125
LS245
LS259
INSTATL
INDATAL
INPARAL
CHBIT0
CHBIT1
RDYL
START
INSTATL
HARD
HAR9
HAR8
HAR7
HAR6
HAR5
HAR4
HAR3
HAR2
HAR1
HAR0
HZORL
HZOWL
HAEN
HD3
HD2
HD1
HD0
HD7
HD6
HD5
HD4
HEO
HRESET
A21
A22
A23
A24
A25
A26
A27
A28
A29
A30
A31
A9
A8
A7
A6
A5
A4
A3
A2
A1
A0
B3
B2
B1
B0
EXU
AURORA
3-2-90

SPECIFICATIONS

At T = 25C and V_R = 0v unless otherwise indicated.

Parameter	ETX 2000			ETX 3000			Units
	Min.	Typ.	Max.	Min.	Typ.	Max.	
Spectral Response	0.8		1.7	0.8		1.7	μm
Responsivity @ 0.85 μm		0.15			0.15		A/W
@ 1.30 μm	0.65	0.80		0.65	0.80		A/W
@ 1.55 μm	0.75	0.90		0.75	0.90		A/W
Shunt Resistance @5mV	0.1	0.2		.04	.08		MΩ
NEP @1.55 μm		0.3			0.5		$pW/(Hz)^{1/2}$
Capacitance		600			1000		pF
Cooler Current*		1.1	1.5		1.1	1.5	A
Cooler Voltage*		1.2	2.0		1.2	2.0	V
Shunt Resistance* @5mV, @-25CV	1			0.4			MΩ

*TE option only

MAXIMUM RATINGS

Parameter	ETX 2000	ETX 3000	Unit
Reverse Voltage	5	3	V
Reverse Current	1	1	mA
Forward Current	100	100	mA
Operating Temperature	-40/+85		°C
Storage Temperature	-60/+125		

OPTIONS

- Ceramic Subcarriers
- Screened minimum responsivity at 0.85 μm.

DISCLAIMER

4-87-05

Preliminary Specifications

ETX 2000T5/TE

ETX 3000T5/TE

EPITAXX

Large Area InGaAs Planar Photodiodes

DESCRIPTION

ETX 2000 and ETX 3000 are large area InGaAs planar PIN photodiodes intended for fiber optics and infrared instrumentation.

They are available in TO-5 hermetic packages (type T5) or mounted on a thermoelectric cooler in a TO-66 package (type TE).

The photosensitive diameters are 2 and 3 mm, respectively.

FEATURES

- High Reliability
- High Shunt Resistance
- High Responsivity at 1.3 and 1.5 μm
- Optional selection for visible response

DIMENSIONS

T5

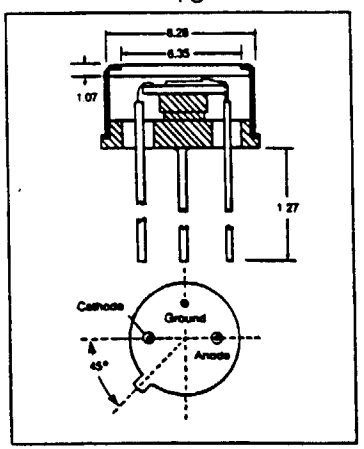

TE

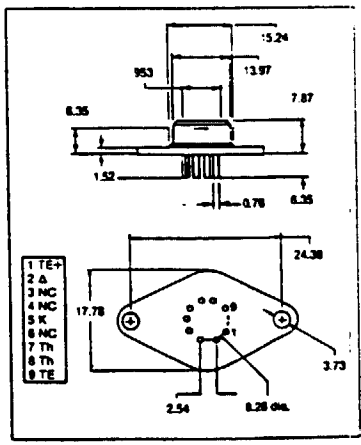

DIMENSIONS IN MM

3490 U.S. ROUTE 1 ■ PRINCETON, NJ 08540 ■ (609) 452-1188 ■ TLX: 759363 ■ FAX: (609) 452-0824

GaAlAs Light Emitting Diode — HFE4003

TYPICAL PERFORMANCE CURVES

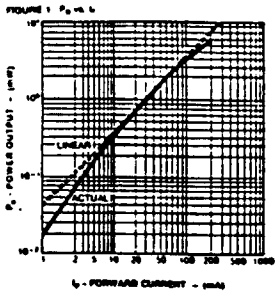

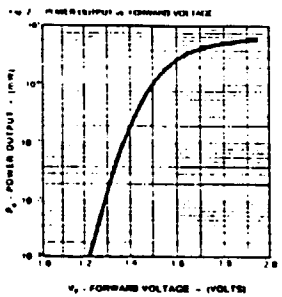

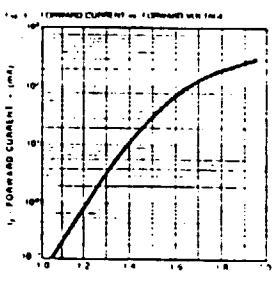

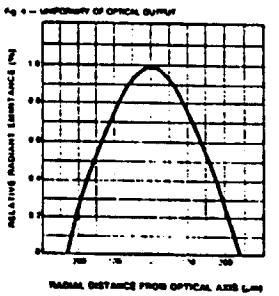

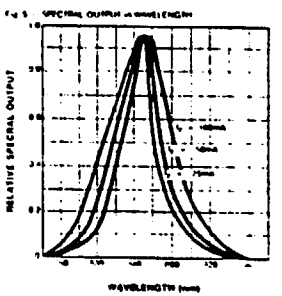

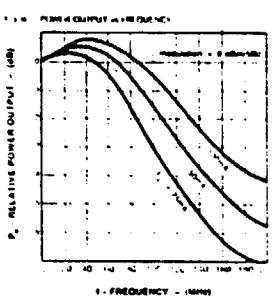

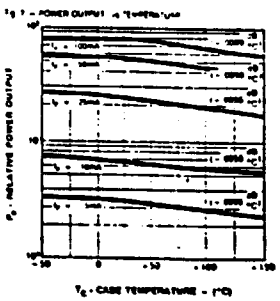

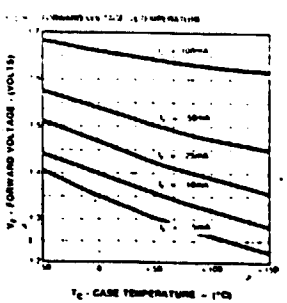

RECOMMENDATIONS

The HFE4003 LED is designed for use with fiber optic receptacles which align the optical axis of the component to the axis of the optical fiber by press fitting the ribbed plastic component cap into the receptacle. Honeywell supplies this part mounted in a variety of receptacles to fit your application. For information on part numbers see page 118 or contact a Honeywell representative for ordering information.

TABLE 1. FIBER COUPLED POWER

Fiber Core Diameter	Fiber Core Index	Numerical Aperture	Typical Coupled Power @ I_F = 100mA		
			-.X22	-.X23	-.X24
50µm	Graded	0.20	10µW	20µW	30µW
85µm	Graded	0.25	30µW	60µW	90µW
100µm	Graded	0.29	100µW	125µW	165µW
200µm	Step	0.40	530µW	700µW	950µW
300µm	Aperture	0.25	750µW	1000µW	1550µW
Total Power Output		-	2.0mW	3.1mW	3.3mW

HFE4003 - GaAlAs Light Emitting Diode

PACKAGE CONFIGURATION

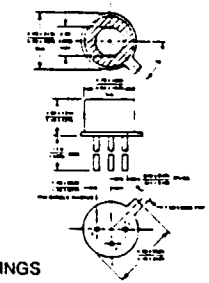

FEATURES

- SWEET SPOT package design for efficient fiber coupling
- Optimized for high power output
- Exceptional linearity for analog transmission
- High reliability
- Replaces SE3362 and SE3352

DESCRIPTION

The HFE4003 is a high radiance GaAlAs IR LED optimized for coupling to a variety of fibers. The unique LED chip design combines high power coupling, with wide bandwidth operation. The peak wavelength is matched for use with Honeywell silicon detectors and receivers.

ABSOLUTE MAXIMUM RATINGS

Storage temperature	-65°C to +150°C
Case operating temperature	-55°C to +125°C
Lead solder temperature	260°C, 10 seconds
Continuous forward current	150mA
Reverse voltage	1V@10µA
Case - cathode (anode) voltage	125 Volts

Notes 1: Anode and Cathode insulated from case
2: Pin 1 — Anode (P-type)
Pin 2 — Cathode (N-type)
Pin 3 — Case (ground)
3 Dimensions in Millimeters (inches)

ELECTRO-OPTICAL CHARACTERISTICS (T_{CASE} = 25°C)

Parameter	Test Condition	Symbol	Dash #	Min	Typ	Max	Units
Forward Voltage	I_F = 100mA	V_F		—	1.6	2.0	Volts
Reverse Voltage	I_R = 10µA	BVR		1.0	5.0		Volts
Series Resistance	DC	r_s			2.0		ohms
Device Capacitance	V_R = 0V, f = 1MHz	C			70		pF
Fiber Coupled Power	I_F = 100mA						
	Fiber Core Diameter = 50µm	P_{OC}	-X22	5	7		µW
	Fiber NA = 0.20	P_{OC}	-X23	10	15		µW
	Fully graded index	P_{OC}	-X24	20	25		µW
	See Note 1 and 2, Table 1						
Spectral Bandwidth		Δλ		50			
Response Time	10-90%, 1V Prebias	t_r			2.5	6.0	ns
	100mA peak	t_f			4.5	6.0	ns
Analog Bandwidth	I_F = 100mA dc, sinusoidal modulation, OdBm/50Ω	BWE			150		MHz
Peak Wavelength	I_F = 100mAdc	λp			850		nm
P_O Temp. Coefficient	I_F = 100mA	$\Delta P_O/\Delta T$			-.010		dB/°C
Thermal Resistance	Heat Sinked	θ			150		°C/w
	No Heat Sink	θ			300		°C/w

Notes 1: The HFE4003 product is tested using a 50µm core fiber located in a V-groove fixture. The fiber is mechanically centered with respect to the can's outside diameter. Actual coupled power values may vary due to mechanical alignment procedures and/or receptacle and fiber tolerances.

2: The three digit dash numbers specify hermeticity and power output. The first digit is zero for standard devices, one for hermetically tested devices. The third digit specifies power output range. Example — Hermetic device with 10µW minimum power output is numbered HFE4003-123.

MOTOROLA
SEMICONDUCTOR
TECHNICAL DATA

Fiber Optics — 100 MHz Family Photo Detector
Diode Output

MFOD1100

HERMETIC FAMILY FIBER OPTICS PHOTO DETECTOR DIODE OUTPUT

. . . designed for infrared radiation detection in high frequency Fiber Optics Systems. It is packaged in Motorola's hermetic TO-206AC (TO-52) case, and it fits directly into standard fiber optics connectors. The metal connectors provide excellent RFI immunity. Major applications are: CATV, video systems, M68000 microprocessor systems, industrial controls, computer and peripheral equipment, etc.

- Fast Response — 1 ns Max @ 5 Volts
- Analog Bandwidth (−3 dB) Greater Than 250 MHz
- Performance Matched to Motorola Fiber Optics Emitters
- TO-206AC (TO-52) Package — Small, Rugged, and Hermetic
- Compatible with AMP #228756-1, Amphenol #905-138-5001 and Radiall #F086600380 Receptacles Using Motorola Plastic Alignment Bushing MF0A06 (Included)

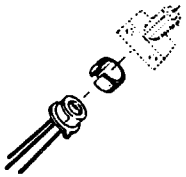

CASE 210A-01
METAL

MAXIMUM RATINGS (T_A = 25°C unless otherwise noted)

Rating	Symbol	Value	Unit
Reverse Voltage	V_R	50	Volts
Total Device Dissipation @ T_A = 25°C Derate above 25°C	P_D	50 0.5	mW mW/°C
Operating Temperature Range	T_A	−55 to +125	°C
Storage Temperature Range	T_{stg}	−65 to +150	°C

ELECTRICAL CHARACTERISTICS (T_A = 25°C)

Characteristic	Symbol	Min	Typ	Max	Unit
Dark Current (V_R = 5 V, R_L = 1 M, H = 0, Figure 2)	I_D	—	—	1	nA
Reverse Breakdown Voltage (I_R = 10 μA)	$V_{(BR)R}$	50	—	—	Volts
Forward Voltage (I_F = 50 mA)	V_F	—	0.7	1	Volts
Total Capacitance (V_R = 5 V, f = 1 MHz)	C_T	—	—	2.5	pF
Noise Equivalent Power	NEP	—	50	—	fW/√Hz

OPTICAL CHARACTERISTICS (T_A = 25°C)

Responsivity @ 850 nm (V_R = 5 V, P = 10 μW, Figure 3, 5)	R	0.3	0.35	—	μA/μW
Response Time @ 850 nm (V_R = 5 V)	t_r, t_f	—	0.5	1	ns
Effective Input Port Diameter (Figure 4)	—	—	300 0.012	—	Microns Inches
10 dB (90%) Numerical Aperture of Input Port (Figure 4)	NA	—	0.4	—	—

TYPICAL CHARACTERISTICS

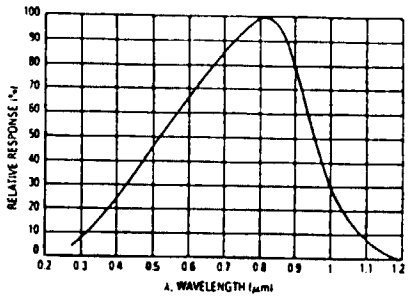

Figure 1. Relative Spectral Response

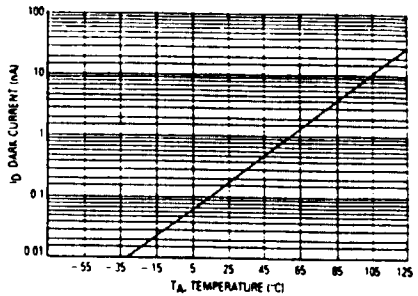

Figure 2. Dark Current versus Temperature

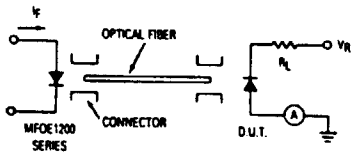

Figure 3. Responsivity Test Configuration

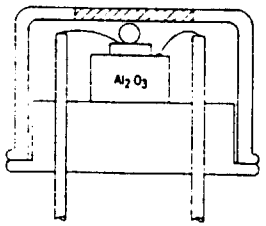

Figure 4. Package Cross Section

OUTLINE DIMENSIONS

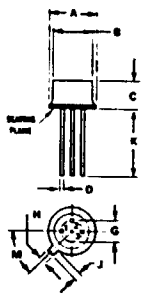

NOTES
1. PIN 2 INTERNALLY CONNECTED TO CASE
2. LEAD POSITIONAL TOLERANCE AT SEATING PLANE
3. DIMENSIONS A AND B ARE DATUMS AND T IS A DATUM PLANE

STYLE:
PIN 1 ANODE
2 CATHODE
3 CASE

DIM	MILLIMETERS MIN	MILLIMETERS MAX	INCHES MIN	INCHES MAX
A	5.31	5.84	0.209	0.230
B	4.65	4.70	0.183	0.185
C	3.12	3.38	0.123	0.133
D	0.41	0.48	0.016	0.019
G	2.54 BSC		0.100 BSC	
H	0.99	1.17	0.039	0.046
J	0.84	1.72	0.033	0.068
K	12.70	—	0.500	—
M	45° BSC		45° BSC	

CASE 210A-01
METAL